Jeffrey R. Carpenter[1]
Eawag, Swiss Federal Institute of
Aquatic Science and Technology,
Surface Waters – Research and Management,
Kastanienbaum 6047, Switzerland;
Department of Geology and Geophysics,
Yale University,
New Haven, CT 06520-8109
e-mail: jeffcarp@gmail.com

Edmund W. Tedford
Marine Science Institute,
University of California, Santa Barbara,
Santa Barbara, CA 93106-9620
e-mail: ttedford@eos.ubc.ca

Eyal Heifetz
Department of Geophysical,
Atmospheric and Planetary Sciences,
Tel Aviv University,
Tel Aviv 69978, Israel;
Department of Meteorology (MISU),
Stockholm University,
Stockholm SE-106 91, Sweden
e-mail: eyalh@cyclone.tau.ac.il

Gregory A. Lawrence
Department of Civil Engineering,
University of British Columbia,
Vancouver, BC, V6T 1Z4, Canada
e-mail: lawrence@civil.ubc.ca

Instability in Stratified Shear Flow: Review of a Physical Interpretation Based on Interacting Waves

Instability in homogeneous and density stratified shear flows may be interpreted in terms of the interaction of two (or more) otherwise free waves in the velocity and density profiles. These waves exist on gradients of vorticity and density, and instability results when two fundamental conditions are satisfied: (I) the phase speeds of the waves are stationary with respect to each other ("phase-locking"), and (II) the relative phase of the waves is such that a mutual growth occurs. The advantage of the wave interaction approach is that it provides a physical interpretation to shear flow instability. This paper is largely intended to purvey the basics of this physical interpretation to the reader, while both reviewing and consolidating previous work on the topic. The interpretation is shown to provide a framework for understanding many classical and nonintuitive results from the stability of stratified shear flows, such as the Rayleigh and Fjørtoft theorems, and the destabilizing effect of an otherwise stable density stratification. Finally, we describe an application of the theory to a geophysical-scale flow in the Fraser River estuary.
[DOI: 10.1115/1.4007909]

1 Introduction

Within the geophysical sciences, shear instability is known to be an important cause of turbulence and mixing in the atmosphere and oceans. Since oceanic and atmospheric flows are generally density stratified, the instability process often involves the interplay of shear and density stratification. The first step in the study of a stratified shear flow is to perform a linear stability analysis to determine whether small perturbations applied to the flow will grow in time. However, the results of stability analyses can often be nonintuitive, and one would hope that a consistent physical interpretation of instability can help explain these results.

One such physical interpretation, which is the focus of this paper, is based on the idea that two otherwise stable waves that exist in the flow may interact to produce instability. This physical interpretation can be used to explain and understand many general results from what can be a mathematically involved stability analysis. Some of the highlights that we present in this paper are (i) a physical interpretation of the Rayleigh and Fjørtoft stability theorems, (ii) the effective extension of these theorems to stratified flows, and (iii) a general classification of instabilities that arise in stratified shear flows based on three fundamental types of wave interactions.

In this paper, we review and consolidate previous work on the wave interaction interpretation of shear instability. The primary goal is to provide a physical understanding of the instability process, and we shall present the review in a fashion that serves as a basic introduction to the wave interaction mechanism. It is not intended to be an exhaustive review of the literature; we focus mainly on understanding the stability properties of piecewise-linear profiles, since this is the easiest possible geometry to apply the wave interaction approach. However, we also describe the extension to more realistic smooth profiles, as well as the application to geophysical flows.

To our knowledge, no review has been written that outlines the wave interaction interpretation, although this has been done in the case of an interpretation in terms of critical layer over-reflection [1]. Furthermore, the classic texts of Drazin and Reid [2] and Betchov and Criminale [3], as well as the more recent text of Schmid and Henningson [4], do not include a discussion of this important physical interpretation of shear flow instability. We begin with a summary of the necessary background theory (Sec. 2), then a description of the basic mechanism of the wave interaction interpretation (Sec. 3). This is followed by the application of this approach to understanding instability in homogeneous flows (Sec. 4), which contains an interpretation of the well-known Rayleigh and Fjørtoft conditions. Stratified flows are analyzed in Sec. 5, where we describe a general classification of the possible instabilities, as well as the application to geophysical flows. A summary is given in the final section along with a discussion of the more recent applications and advancements of the theory.

2 Background Theory

2.1 Linear Stability Analysis and the Taylor–Goldstein Equation. A linear stability analysis involves determining the fate of small disturbances, or perturbations, to a background flow state. If the perturbations are found to grow in time, then the background state is said to be unstable, and we expect to see a different

[1]Corresponding author.

Manuscript received May 20, 2011; final manuscript received October 17, 2012; published online January 23, 2013. Editor: Harry Dankowicz.

type of flow emerge. This is the classic temporal approach to assessing the stability of the flow: perturbations are taken to be sinusoidal in the along-flow direction (x), and the evolution in time (t) is sought. In the case of stratified shear flow, the background state corresponds to the basic vertical profiles of horizontal velocity $U(z)$ and density $\bar{\rho}(z)$. Since the perturbations are assumed to be small, we are justified in neglecting the products of any perturbations that appear in the equations of motion. Once the appropriate simplifications are made to the equations of motion, a linear equation is left that describes the evolution of the perturbations in time.

Since our focus is on the mechanism by which shear and stratification may act to produce instability, we neglect all other processes that complicate the analysis. These include:

(1) viscosity
(2) diffusion of mass
(3) compressibility
(4) inertial effects of density variations (i.e., we make the Boussinesq approximation)
(5) rotation
(6) three-dimensional motions
(7) the presence of solid boundaries

All of the above may be included in the analysis if desired, but in many important cases they do not significantly change the results. We refer the interested reader to Refs. [5,6] for the inclusion of viscosity and diffusion, Ref. [7] for compressibility effects, Refs. [8,9] for a non-Boussinesq treatment, as well as Refs. [10,11] for including rotation, and Refs. [12,13] for three-dimensional effects.

With the above simplifications, we can write the conservation of momentum as

$$\rho_0\left(\frac{\partial \mathbf{u}}{\partial t}+\mathbf{u}\cdot\nabla\mathbf{u}\right)=-\nabla p-\rho g\mathbf{k} \tag{1}$$

with ρ_0 a constant reference density, p the pressure, ρ the density, g the gravitational acceleration, and $\mathbf{k}$ the unit vector in the vertical (z) direction. We also use an equation that expresses the conservation of fluid density by

$$\frac{\partial \rho}{\partial t}+\mathbf{u}\cdot\nabla\rho=0 \tag{2}$$

where we have also used the incompressible continuity equation

$$\nabla\cdot\mathbf{u}=0 \tag{3}$$

The first step in understanding instability in stratified shear flow is to express the conservation of momentum in terms of the vorticity $\mathbf{q}\equiv\nabla\times\mathbf{u}$, and since we are assuming a two-dimensional velocity field $\mathbf{u}=(u,w)$, the vorticity reduces to a scalar quantity given by $q=\partial u/\partial z-\partial w/\partial x$. Vorticity plays a central role in the physical interpretation of shear instability. This is due to the fact that, in the case of homogeneous flows (i.e., without density variations), vorticity is a conserved quantity. This is expressed mathematically in the conservation of vorticity equation

$$\frac{\partial q}{\partial t}+u\frac{\partial q}{\partial x}+w\frac{\partial q}{\partial z}=0 \tag{4}$$

formed by taking the curl of Eq. (1), which simply states that any changes in q that occur at some fixed point, are due entirely to the advection of existing vorticity gradients past this point. There is no creation or destruction of q, and any q that is present must have come from the initial condition. Since any changes in vorticity that occur are kinematic we refer to this as the kinematic vorticity of the shear layer, after Holmboe [14]. When density stratification is present, q may be generated by horizontal density gradients (tilted isopycnals), and Eq. (4) is now modified with a source term included on the right hand side, viz.

$$\frac{\partial q}{\partial t}+u\frac{\partial q}{\partial x}+w\frac{\partial q}{\partial z}=\frac{g}{\rho_0}\frac{\partial \rho}{\partial x} \tag{5}$$

This mechanism of vorticity generation is referred to as baroclinic, and may be thought of as the vorticity signature of the buoyancy forces.

We now use this principle to formulate the Taylor–Goldstein (TG) equation, which governs the stability of stratified shear flows, subject to the simplifications (1)–(6) listed above. The steps taken are as follows:

(1) Express all variables in terms of the background flow and a small superimposed perturbation, denoted by a $\tilde{}$, i.e.,

$$u=U(z)+\tilde{u},\quad w=\tilde{w},\quad q=Q(z)+\tilde{q},\quad \rho=\bar{\rho}(z)+\tilde{\rho} \tag{6}$$

Here the perturbation quantities are all functions of (x, z, t).

(2) Substitute the form Eq. (6) into the vorticity Eq. (5) and neglect products of perturbation quantities since they are presumed to be small. This gives

$$\frac{D\tilde{q}}{Dt}=-\tilde{w}\frac{dQ}{dz}+\frac{g}{\rho_0}\frac{\partial\tilde{\rho}}{\partial x} \tag{7}$$

where we use $D/Dt\equiv\partial/\partial t+U\partial/\partial x$ here, and throughout the paper, to represent a linearized material derivative. This is an equation for the generation and advection of *perturbation* vorticity, $\tilde{q}$. It can be seen that a new source term is present on the right hand side that gives the generation of $\tilde{q}$ from the background vorticity Q.

(3) Eliminate $\tilde{\rho}$ by using the linearized density conservation Eq. (2)

$$\frac{D\tilde{\rho}}{Dt}=-\tilde{w}\frac{d\bar{\rho}}{dz} \tag{8}$$

(4) Utilize a stream function representation of the perturbation velocity field such that

$$\tilde{u}\equiv\frac{\partial\tilde{\psi}}{\partial z}\quad\text{and}\quad\tilde{w}\equiv-\frac{\partial\tilde{\psi}}{\partial x} \tag{9}$$

which ensures that the incompressible continuity Eq. (3) is satisfied.

(5) Since the resulting equation is linear with coefficients that depend only on z, we can take the normal mode form of

$$\tilde{\psi}(x,z,t)=\hat{\psi}(z)e^{ik(x-ct)} \tag{10}$$

for the stream function solution. This form of solution consists of perturbations that are sinusoidal in x with wavenumber $k=2\pi/\lambda$, where λ is the wave length, and have some vertical structure that is given by $\hat{\psi}(z)$. Note that this normal mode form applies also to the other perturbation quantities in Eq. (6).

(6) After substituting in the normal mode form of Eq. (10) into Eq. (7) and simplifying, we arrive at

$$\hat{\psi}''-\left[\frac{U''}{U-c}-\frac{N^2}{(U-c)^2}+k^2\right]\hat{\psi}=0 \tag{11}$$

where we have used primes to represent ordinary differentiation with respect to z, and the squared buoyancy frequency $N^2 \equiv -g\bar{\rho}'/\rho_0$.

Equation (11) is the Taylor–Goldstein (TG) equation in the standard form, but more insight into the equation can be gained by rearranging into the following:

$$\underbrace{(U-c)\overbrace{(\hat{\psi}''-k^2\hat{\psi})}^{\text{perturbation vorticity}}}_{\text{vorticity generation}} = \underbrace{U''\hat{\psi}}_{\text{kinematic generation}} - \underbrace{\frac{N^2}{U-c}\hat{\psi}}_{\text{baroclinic generation}} \tag{12}$$

expressing the generation of perturbation vorticity, on the left-hand side, in terms of two source terms: (i) the kinematic generation by vertical displacements of gradients in the background vorticity (U''), and (ii) the production of baroclinic vorticity by tilting of the background density gradient (measured by N^2).

The TG equation describes an eigen-problem for the eigenvalue c and the eigenfunction $\hat{\psi}(z)$. Both of these quantities may have complex values. In the case of complex valued phase speeds $c = c_r + ic_i$, the real part c_r represents the phase speed of the perturbation, while a positive imaginary component c_i indicates an exponential growth of the perturbation in time, with a growth rate given by the imaginary component of the complex frequency $\omega_i = kc_i$.

2.2 An Alternative Formulation. It is helpful to also consider an alternative formulation to expand on our physical interpretation of the TG equation. In particular, to write the perturbation vorticity balance without assuming a normal mode form (i.e., as in Eq. (10)). First, we define a field $\tilde{\eta}(x,z,t)$, that gives the vertical displacement of any material contour from its background value. In this paper, we will often speak of the vertical displacement of the conserved scalar fields of density and kinematic vorticity. Since we are using a linear theory, the perturbations of kinematic vorticity $\tilde{q}_K$, and density $\tilde{\rho}$ can be written as linear expansions from the background profiles via

$$\tilde{q}_K = -Q'\tilde{\eta} = -U''\tilde{\eta} \tag{13}$$

and

$$\tilde{\rho} = -\bar{\rho}'\tilde{\eta} = \frac{\rho_0}{g}N^2\tilde{\eta} \tag{14}$$

It is clear from Eq. (13) that the kinematic vorticity perturbation is produced from the vertical displacement of the background shear. A $\tilde{q}_K$ budget can therefore be written as

$$\frac{D\tilde{q}_K}{Dt} = -U''\frac{D\tilde{\eta}}{Dt} \tag{15}$$

Likewise, a baroclinic perturbation vorticity $\tilde{q}_B$, can be defined in analogy with Eq. (5) using Eq. (14) to write

$$\frac{D\tilde{q}_B}{Dt} = N^2\frac{\partial\tilde{\eta}}{\partial x} \tag{16}$$

and we see that baroclinic vorticity is generated by the tilting of density surfaces. The total $\tilde{q}$ budget will then be the sum of the kinematic and baroclinic portions with

$$\underbrace{\frac{D\tilde{q}}{Dt}}_{\text{vorticity generation}} = \underbrace{-U''\frac{D\tilde{\eta}}{Dt}}_{\text{kinematic generation}} + \underbrace{N^2\frac{\partial\tilde{\eta}}{\partial x}}_{\text{baroclinic generation}} \tag{17}$$

This equation is the TG equation governing stratified shear flows, and the terms represent the same quantities as in Eq. (12). However, there is one more essential ingredient that links the vertical displacement field with the vorticity field. This is done by relating $\tilde{\eta}$ to the vertical velocity through the kinematic condition

$$\frac{D\tilde{\eta}}{Dt} = \tilde{w} \tag{18}$$

One may think of these two equations, Eqs. (17) and (18), as coupled by first displacing the $Q(z)$ or $N^2(z)$ profiles, thus generating a $\tilde{q}$ field, which then leads to a new $\tilde{w}$, giving a new $\tilde{\eta}$, and so on.

2.3 Stable Waves on a Single Interface. A prerequisite to understanding instability in stratified shear flows is a knowledge of the stable waves that may exist. There are two basic types of waves that each result from one of the two vorticity generation terms of the TG equation (see Eq. (12)): (i) vorticity waves that arise from the kinematic generation term, and propagate on gradients in the background vorticity (U''), and (ii) internal gravity waves that arise from the baroclinic term, which propagate on background density gradients (N^2).

The simplest scenario to examine these two different types of waves, presented by Baines and Mitsudera [15], is one where U is represented by a piecewise-linear profile, with a layered background vorticity (recall $Q = U'$), given by

$$U(z) = \begin{cases} U_\ell, & z \geqslant z_\ell \\ Sz, & z \leqslant z_\ell \end{cases}, \quad \text{and} \quad Q(z) = \begin{cases} 0, & z > z_\ell \\ S, & z < z_\ell \end{cases} \tag{19}$$

where $S = U_\ell/z_\ell$ is the vorticity, or shear in the lower layer, and $\bar{\rho}$ is represented by the layered profile

$$\bar{\rho}(z) = \begin{cases} \rho_0, & z > z_\ell \\ \rho_0 + \Delta\rho, & z < z_\ell \end{cases} \tag{20}$$

These piecewise profiles are sketched in Fig. 1(*a*). The level z_ℓ is referred to as an interface, which may be either a vorticity or density interface depending on the profiles, or both. The advantage of taking these piecewise profiles is because of the simplification that results in the TG equation. Each of the two generation terms has a δ function behavior at the interface level z_ℓ, with $U''(z) = \Delta Q\delta(z-z_\ell)$ and $N^2(z) = g'\delta(z-z_\ell)$, where $\Delta Q = U'(z_\ell^+) - U'(z_\ell^-)$ is the vorticity jump across the interface, and $g' = \Delta\rho g/\rho_0$ is the reduced gravity across the interface with $\Delta\rho > 0$ for stable stratification. In the case of the profiles in Eq. (19) and Fig. 1, $\Delta Q = -S$. We may now write the TG equation as[2]

$$\hat{\psi}'' - k^2\hat{\psi} = 0, \quad \text{for} \quad z \neq z_\ell \tag{21}$$

Recall that perturbations to the vorticity field are given by $\hat{q} = \hat{\psi}'' - k^2\psi$, which now vanishes at all locations except at the level of the interface $z = z_\ell$. This considerably simplified equation expresses the fact that in the background flow of Eqs. (19) and (20), only the interface is responsible for generating perturbations

[2]Here we are neglecting a part of the solution referred to as the continuous spectrum, which is not essential for the purposes of this paper. For more information the reader is referred to Schmid and Henningson [4].

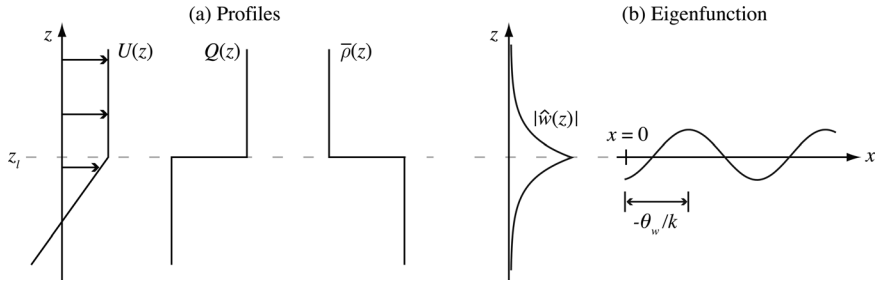

Fig. 1 (*a*) Piecewise profiles used to demonstrate vorticity and internal gravity waves. The interface of density and vorticity is located at z_ℓ. (*b*) The vertical velocity eigenfunction $\hat{w}(z)$ for vorticity and internal gravity waves. Since $\hat{w}(z)$ is generally complex it has both an amplitude $|\hat{w}(z)| = |A|e^{-k|z-z_\ell|}$ and a phase given by $\tan(\theta_w) = \mathrm{Im}(\hat{w})/\mathrm{Re}(\hat{w}) = \mathrm{Im}(A)/\mathrm{Re}(A)$.

to the vorticity field. It is these perturbations that lead to a stable wave motion.

Together with the boundary conditions that $\hat{\psi} \to 0$ as $z \to \pm\infty$, Eq. (21) may be easily solved to give an exponentially decaying stream function for the perturbations away from the interface level, viz.

$$\hat{\psi}(z) = Ae^{-k|z-z_\ell|} \tag{22}$$

Note that this solution decays in such a way to leave the flow irrotational (i.e., vorticity free) everywhere but at the interface, similar to a surface gravity wave [16]. The coefficient, A, is a constant of integration that is generally complex, and represents both the (infinitesimal) amplitude, and the phase of the interfacial wave (see Fig. 1(*b*)). In arriving at this form, we have also imposed the condition that $\hat{\psi}$ be continuous across the level $z = z_\ell$, which corresponds to a continuous vertical velocity. Note that by definition of the stream function $\hat{w} = -ik\hat{\psi}$, so the vertical velocity of the perturbation also has an exponential decay from the interface level (Fig. 1(*b*)). Throughout the paper we will use $\tilde{q}(x)$, $\tilde{w}(x)$, and the vertical displacement of the interface, $\tilde{\eta}(x)$, to describe the structure of the waves.

Propagation characteristics of the waves are contained in the dispersion relation, which relates either the complex phase speed c, or equivalently, the complex frequency $\omega = kc$, to the wavenumber k, i.e., $c = c(k)$ or $\omega = \omega(k)$. This dispersion relation is found by using the stream function solution (Eq. (22)) to integrate the TG equation across the interface at z_ℓ, and leads to the "jump" condition

$$\left[\!\left[(U-c)\hat{\psi}' - U'\hat{\psi}\right]\!\right]_{z_\ell} + \frac{g'_\ell}{U_\ell - c}\hat{\psi}_\ell = 0 \tag{23}$$

where $[\![f]\!]_{z_\ell} \equiv f(z_\ell^+) - f(z_\ell^-)$ indicates a jump across the interface at z_ℓ, and the ℓ subscript refers to evaluation at z_ℓ (e.g., $U_\ell = U(z_\ell)$). Equation (23) is equivalent to imposing a continuous pressure distribution across the interface (see Drazin and Reid [2] for further details). After simplification of the jump condition, we arrive at the dispersion relation

$$U_\ell - c = -\frac{\Delta Q}{4k} \pm \left[\left(\frac{\Delta Q}{4k}\right)^2 + \frac{g'}{2k}\right]^{1/2} \tag{24}$$

where U_ℓ can be seen to cause an advection of the wave by the basic profile. It is helpful to look at two special cases of this dispersion relation: pure vorticity waves, and pure internal gravity waves.

Vorticity Waves. If we let $g' = 0$ so that the flow is homogeneous, the quadratic dispersion relation in Eq. (24) simplifies to a linear relation for what we shall refer to as a *vorticity wave* on a *vorticity interface*, namely,

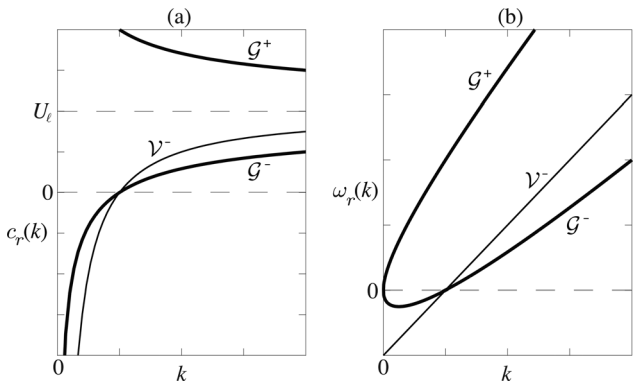

Fig. 2 Dispersion relation for the profiles in Fig. 1 showing (*a*) the phase speed $c_r(k)$, and (*b*) the frequency $\omega_r(k)$ for vorticity and internal gravity waves. The vorticity wave mode shown here has a leftward intrinsic propagation and is denoted by $\mathcal{V}^-$ (thin line), whereas the gravity wave modes are indicated by $\mathcal{G}^\pm$ (thick lines) and have intrinsic propagation in both directions.

$$c_r = U_\ell + \frac{\Delta Q}{2k} \quad \text{and} \quad c_i = 0 \tag{25}$$

It should be noted that the vorticity wave has also been referred to as a 'Rayleigh wave' [14,17] and as a 'counter-propagating Rossby wave' [18–20]. It can be seen to propagate in a single direction that is determined by the sign of the vorticity jump ΔQ, when in a frame of reference moving at the speed of the interface level U_ℓ. In other words, the *intrinsic* propagation speed of the vorticity wave is leftwards in the profile of Fig. 1(*a*). The dispersion relation (Eq. (25)) for the vorticity wave is plotted in Fig. 2. These stable vorticity wave modes shall be denoted by $\mathcal{V}^-$ and $\mathcal{V}^+$, where the $+$ and $-$ superscripts refer to the intrinsic propagation speed with $+$ $(-)$ in the positive (negative) x-direction.

To gain an understanding of the propagation mechanism of the vorticity wave, we plot three important fields in Fig. 3: the vertical displacement of the interface $\tilde{\eta}(x)$, the (kinematic) vorticity perturbation $\tilde{q}(x)$ that it generates, and the resulting vertical velocity at the interface, $\tilde{w}(x, z_\ell)$. Recall that the kinematic vorticity of the shear layer is conserved; therefore, a sinusoidal displacement of the vorticity interface will lead to a sinusoidal distortion of the background vorticity; shear layer vorticity will be moved upwards in the wave crests and downwards in the troughs. This creates a perturbation $\tilde{q}$ that is either in-phase, or 180 deg out-of-phase, with $\tilde{\eta}$, depending on the sign of ΔQ. For the $U(z)$ that we have chosen to show in Fig. 3, $\tilde{q}$ is in-phase with $\tilde{\eta}$. The $\tilde{w}$ that this $\tilde{q}$ sets up has a phase lag of 90 deg, with the largest velocities

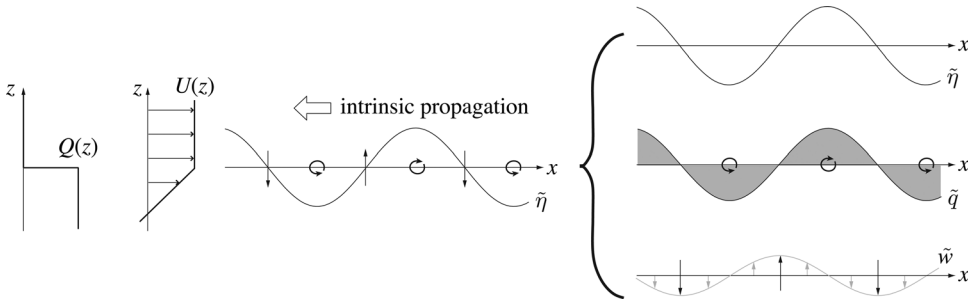

Fig. 3 Structure of the vorticity wave broken down into three important fields: interface displacement $\tilde{\eta}$, vorticity perturbation $\tilde{q}$, and the vertical velocity $\tilde{w}$. These fields are all sinusoidal with wavenumber k and illustrated on the right. Throughout the remainder of the paper we will use the more compact notation shown on the left, with circular arrows denoting crests (clockwise) and troughs (counterclockwise) in $\tilde{q}$ and similarly with the vertical arrows denoting crests and troughs in the $\tilde{w}$-field. These diagrams will be referred to as *wave field diagrams*.

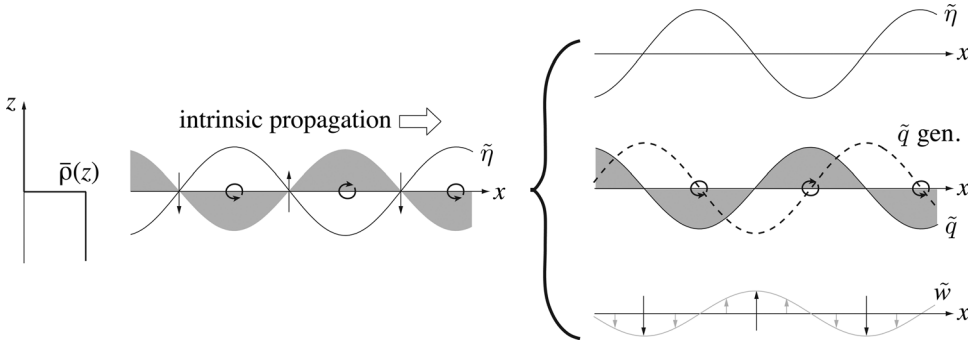

Fig. 4 Structure of the rightward-propagating internal gravity wave broken down into its important fields. The notation is the same as in Fig. 3 except we have also plotted the generation of baroclinic vorticity, described by Eq. (16), as the dashed line. In addition to the rotational arrows, the $\tilde{q}$-field is indicated by the gray shading. This is because once wave interactions are accounted for the $\tilde{q}$-field is not generally directly related to the $\tilde{\eta}$-field, as is the case in the vorticity wave (see Sec. 5).

occurring at the nodes of $\tilde{q}$ and $\tilde{\eta}$. This phase relationship between $\tilde{w}$ and $\tilde{\eta}$ leads to a stable propagating wave, which in the orientation shown in Fig. 3, travels to the left.

We must caution the reader that we have been loose with our description of the perturbation vorticity field $\tilde{q}$, here. Although Fig. 3 does accurately represent the voricity wave, linear theory models the $\tilde{q}$-field as a vortex sheet, where $\tilde{q}$ is concentrated entirely at the interface level, with δ function behavior. This can be seen from Eq. (13) by substituting $U'' = \Delta Q \delta(z - z_\ell)$. In this sense, what we are really referring to is the *strength* of the vortex sheet, which is equivalent to the circulation per wavelength, and is given by $-\Delta Q \tilde{\eta}_\ell$.

Internal Gravity Waves. The second special case of the dispersion relation (Eq. (24)) is obtained by eliminating the vorticity gradient ($U'' = 0$) by setting $\Delta Q = 0$, so that we recover a *density interface* in uniform shear. The resulting *internal gravity waves*, or simply *gravity waves* in short, have a dispersion relation given by

$$c_r = U_\ell \pm \sqrt{\frac{g'}{2k}} \quad \text{and} \quad c_i = 0 \tag{26}$$

which is plotted in Fig. 2. This dispersion relation is equivalent to the classical solution for water waves on the air-water interface when the water depth is much greater than the wavelength (deep water waves), and the Boussinesq approximation is made (see Chap. 7 of Ref. [16]). In this case $g' = \Delta\rho g/\rho_0 \approx 2g$, when ρ_0 is taken as the average density.

Unlike the vorticity interface, there are two gravity wave modes that exist on a single interface, denoted by $\mathcal{G}^{\pm}$, with an intrinsic propagation in both directions (i.e., relative to the interfacial advective velocity U_ℓ). The structure of the $\tilde{\eta}$, $\tilde{q}$, and $\tilde{w}$ fields at the density interface of a rightward-propagating gravity wave is shown in Fig. 4. As opposed to the vorticity wave, the source of $\tilde{q}$ in the internal gravity wave is from the baroclinic generation term of Eq. (12) and Eq. (17). In this case, as the wave propagates past, in a reference frame moving at U_ℓ, vorticity is generated at the nodes of the $\tilde{\eta}$ field where the slope is greatest, and accumulates in the crests and troughs where the generation vanishes. For the rightward-propagating internal gravity wave, the $\tilde{q}$ and $\tilde{w}$ fields are phase shifted by 180 deg from Fig. 3. Note that the dispersion relation in Eq. (26) is independent of the strength of the shear that is present in the background $U(z)$ profile since no perturbation is generated by its vertical displacement (i.e., $U'' = 0$); however, this is only true when the Boussinesq approximation is made [9].

3 The Wave Interaction Interpretation of Instability

With knowledge of the two fundamental stable wave motions that may exist in stratified shear flows, namely the vorticity wave and the internal gravity wave, we can now examine how two waves may interact to produce instability. In this section, we shall demonstrate that there are two essential conditions that must be satisfied by the otherwise stable waves in order for instability to occur. These conditions are

Condition I: the phase speeds of the waves are stationary with respect to each other ('phase-locking').

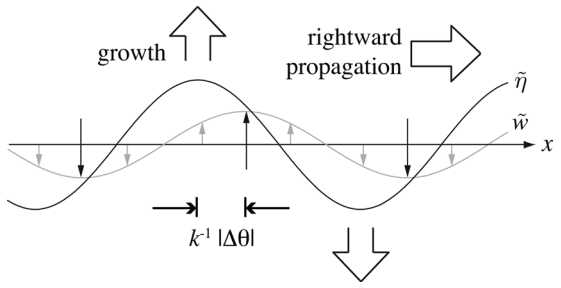

Fig. 5 Illustration of the relationship between the $\tilde{\eta}$ and $\tilde{w}$ fields in a growing and rightward-propagating interfacial wave

Condition II: the relative phase of the waves is such that mutual growth of the interfaces occurs.

In order to demonstrate this, consider first a single interface located at height z_ℓ, with a vertical displacement $\tilde{\eta}_\ell = \tilde{\eta}(z_\ell, t) = \mathrm{Re}\{A_\eta(t)e^{i\theta_\eta(t)}e^{ikx}\}$. We now subject this interface to a sinusoidal vertical velocity field that has the value $\tilde{w}_\ell = \mathrm{Re}\{A_w e^{i\theta_w}e^{ikx}\}$. This $\tilde{w}$-field may be thought of as the $\tilde{w}$-field due to the intrinsic propagation of the interface at z_ℓ plus the $\tilde{w}$-field of some other distant wave which it is interacting with. The evolution in time of the interface can be found from the linearized kinematic condition in Eq. (18), relating $\tilde{\eta}$ to $\tilde{w}$. Substituting the sinusoidal forms above, we can derive an expression for both the growth rate and the phase speed of the interface as,

$$\text{Growth Rate:} \quad \frac{\dot{A}_\eta}{A_\eta} = \frac{A_w}{A_\eta}\cos(\Delta\theta) \tag{27}$$

$$\text{Phase Speed:} \quad -k^{-1}\dot{\theta}_\eta = U_\ell - k^{-1}\frac{A_w}{A_\eta}\sin(\Delta\theta) \tag{28}$$

where the dot represents ordinary differentiation with respect to t, and $\Delta\theta = \theta_w - \theta_\eta$ denotes the phase difference between the two fields. This phase difference determines the growth and propagation of the displacement field. When $\tilde{w}_\ell$ and $\tilde{\eta}_\ell$ are in-phase ($\Delta\theta = 0$) there is pure growth of the interface, with no intrinsic propagation. Alternatively, if the phase difference is ± 90 deg ($\Delta\theta = \pm\pi/2$) then the interface will simply propagate with no change in amplitude, with the direction of propagation determined by whether the phase difference is leading or lagging. This was the case for the stable waves of Sec. 2.3 (e.g., Fig. 3).

The relationship between $\tilde{w}$ and $\tilde{\eta}$, described mathematically by Eqs. (27) and (28), is illustrated in Fig. 5, where a growing, rightward-propagating wave is shown. Once the $\tilde{\eta}$ and $\tilde{w}$ fields at a particular interface are known, one can see from a simple visual inspection, as shown in Fig. 5, both the direction of intrinsic propagation and the growth or decay of the interface: if $\tilde{w}$ has a component that is upwards in the $\tilde{\eta}$-crests then wave growth will occur, similarly if $\tilde{w}$ is upwards at the positively sloping $\tilde{\eta}$-nodes then the intrinsic propagation will be leftward. The opposite relations are also true: if $\tilde{w}$ has a component that is downwards in the $\tilde{\eta}$ crests then there is a decay, and if $\tilde{w}$ is downwards at a positively sloping $\tilde{\eta}$ node the intrinsic phase speed is rightwards. These wave field diagrams will be used throughout the paper to illustrate the wave interactions, and to gain a physical understanding of shear instability in homogeneous and stratified flows.

It is important to note that the conditions I and II apply to the *normal mode* instability of two interacting interfacial waves, whereas Eqs. (27) and (28) apply to any sinusoidal interface. In fact, one could easily construct two interacting interfacial waves, each with arbitrary $\tilde{w}$- and $\tilde{\eta}$-fields, and then apply Eqs. (27) and (28) to evaluate their phase speed and growth rates. However, this will not be a normal mode unless the growth rate and phase speed of each interface are equal. Then we may write $\dot{A}_\eta/A_\eta = \omega_i$ and $-k^{-1}\dot{\theta}_\eta = c_r$ for both interfaces. We can therefore see that the normal modes are a very special configuration, and that wave interactions can be a powerful tool to interpret transient non-normal growth in shear flows [19,21].

4 Homogeneous Shear Flows

4.1 Unstable Interaction: The Shear Layer. The first case of interacting waves that we examine will be the piecewise shear layer [22], since it serves to illustrate how two waves may interact to produce instability. This discussion follows those given previously in the pioneering papers of Garcia [23] and Holmboe [14], as well as more recent descriptions in Refs. [15,18–20,24].

In much of the analysis to follow, it will be convenient to use certain length and velocity scales to nondimensionalize the important variables. To make the notation more convenient, we shall henceforth use an asterisk to denote dimensional variables, and variables without an asterisk will be understood as dimensionless. For example, we can therefore define dimensionless quantities as follows,

$$U = \frac{U_*}{V_*}, \quad z = \frac{z_*}{L_*}, \quad \hat{\psi} = \frac{L_*}{V_*}\hat{\psi}_*$$
$$c = \frac{c_*}{V_*}, \quad \omega = \frac{L_*}{V_*}\omega_*, \quad k = k_* L_*, \ldots$$

where L_* and V_* represent length and velocity scales that are to be defined for each particular problem of interest.

The shear layer consists of two vorticity interfaces of opposite sign that are separated by a height h_*, over which the horizontal

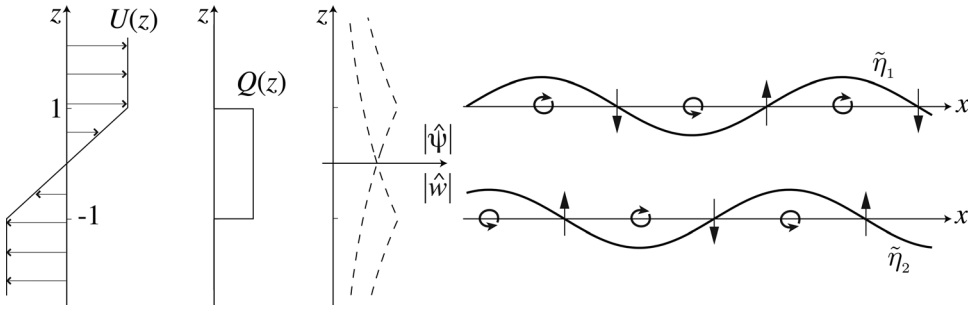

Fig. 6 The piecewise shear layer profile on left along with the eigenfunction amplitude of the two interface contributions to the total eigenfunctions $|\hat{w}(z)|$ and $|\hat{\psi}(z)|$, which are related by $\hat{w} = -ik\hat{\psi}$. The wave field diagram illustrating the unstable interaction of vorticity waves is shown on the right for the particular value of $k = 0.4$, corresponding to the maximum growth rate. As in Fig. 3, the vertical arrows indicate the peaks and troughs in the $\tilde{w}$-fields at each interface, due only to the displacement of that interface. In addition, we also show the vorticity $\tilde{q}$ and displacement $\tilde{\eta}$ of each interface.

velocity changes by an amount ΔU_* (Fig. 6). In the nondimensionalization we shall take $L_* = h_*/2$ and $V_* = \Delta U_*/2$ so that the profiles can be written as

$$U(z) = \begin{cases} 1, z \geqslant 1 \\ z, |z| \leqslant 1 \\ -1, z \leqslant -1 \end{cases} \quad \text{and} \quad Q(z) = \begin{cases} 0, & |z| > 1 \\ 1, & |z| < 1 \end{cases} \tag{29}$$

in the new dimensionless coordinate system, as shown in Fig. 6. The stability properties of the shear layer are found by solving the TG equation, which reduces to the simple form of Eq. (21) except at the two vorticity interfaces at $z = \pm 1$, where the kinematic vorticity generation term has δ function behavior. The eigenfunction is simply the sum of two exponentially decaying interfaces, i.e.,

$$\hat{\psi}(z) = Ae^{-k|z-1|} + Be^{-k|z+1|} \tag{30}$$

as shown in Fig. 6. The two complex valued coefficients A and B represent the unknown amplitudes and phases of the two interfacial vorticity waves, and are determined by integrating the TG equation across the interface locations at $z = \pm 1$. In the case of a pure vorticity interface this leads to the "jump" condition,

$$\left[\!\left[(U - c)\hat{\psi}' - U'\hat{\psi} \right]\!\right]_{z_\ell} = 0 \tag{31}$$

The dispersion relation is found by solving the linear system in A, B from the jump conditions at each interface, and is plotted in Fig. 7.

To understand the wave behavior seen in the dispersion relation, consider the hypothetical case in which both vorticity wave modes are in isolation from one another, and therefore do not interact. The dispersion relation is then given by

$$\mathcal{V}_1^- : \omega = k - 1/2 \quad \text{and} \quad \mathcal{V}_2^+ : \omega = -k + 1/2 \tag{32}$$

for the upper and lower vorticity waves, indicated by the subscripts 1 and 2, and are shown by the gray lines on Fig. 7. The assumption that the upper and lower wave modes are in isolation is accurate when k becomes large, which can be seen from Fig. 7 to be approximately satisfied for $k \gtrsim 1$. In this case, the dimensional vertical distance between the interfaces, h_*, is large compared to the wavelength; the exponential decay of the eigenfunctions (wave evanescence) is so great that the waves do not 'feel' each other's presence. At these relatively large k, the two interacting stable wave modes, denoted by $\mathcal{S}_1$ and $\mathcal{S}_2$ in Fig. 7, are nearly indistinguishable from the isolated vorticity waves $\mathcal{V}_1^-$, and $\mathcal{V}_2^+$.

As k decreases, the vertical (exponential) decay of the eigenfunctions associated with each interface becomes less, and the interaction of the waves becomes stronger as they begin to feel each others presence. In addition to the increasing strength of the $\tilde{w}$-field felt by each vorticity interface from its neighbor, as k decreases towards 0.5 the phase speeds (inferred from ω_r) of the isolated waves naturally approach one another (Fig. 7). Both the interaction and the natural convergence of the phase speeds work together to eventually bring the waves to a state where they are stationary relative to each other at $k = 0.64$—referred to as 'phase-locking'. As k is decreased further, phase-locking can be maintained even though the isolated phase speeds are generally not equal (except at $k = 0.5$) due to the interaction between the waves. An induced phase speed exactly canceling the intrinsic propagation speed is maintained by adjusting the phase difference between waves (see Eq. (28)). Therefore, condition (I) from Sec. 3 is satisfied for the band $0 < k < 0.64$, through adjustments in the relative phase difference of the waves. Note that this phase difference is exactly 45 deg at $k = 0.5$ because no induced phase speed adjustment due to wave interactions is needed to cause phase locking—the waves are naturally phase locked when in isolation (i.e., the crossing of the gray lines $\mathcal{V}_1^-$ and $\mathcal{V}_2^+$ at $k = 0.5$ in Fig. 7).

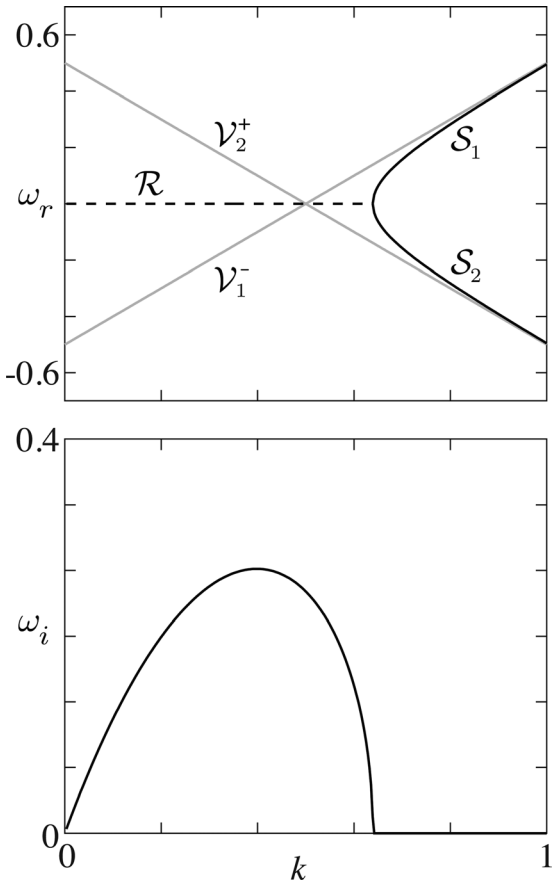

Fig. 7 Dispersion relation for the piecewise shear layer. Upper panel shows the real frequency $\omega_r(k)$ of the dispersion relation with the dashed line indicating unstable ($\mathcal{R}$) modes, solid lines denote the two stable ($\mathcal{S}$) modes, and the gray lines correspond to the isolated vorticity waves of the upper ($\mathcal{V}_1^-$) and lower ($\mathcal{V}_2^+$) interfaces. The bottom panel shows the growth rate $\omega_i(k)$ of the unstable mode.

As a special case, we examine the wave number of maximum growth rate at $k = 0.4$, where the wave fields of the upper and lower interfaces are shown in Fig. 6. In this configuration, the vorticity waves would propagate past each other if there were no interaction between them. Focusing on the upper interface, we see that it has a propagation that is leftwards when in isolation ($\mathcal{V}_1^-$ at $k = 0.4$ in Fig. 7). However, this propagation is counteracted by the changes in phase speed induced by the $\tilde{w}_2$-field of the lower vorticity wave. If we recall the discussion of Eqs. (27) and (28) in the previous section, this can be seen directly from the wave-field diagram in Fig. 6. Since the $\tilde{w}_2$-field of the lower wave has a component that is upwards at the negatively-sloping nodes of $\tilde{\eta}_1$ it induces a rightwards propagation. This interaction is just sufficient to bring the waves stationary with respect to one another. The wave-field diagram in Fig. 6 demonstrates that condition (II) is also satisfied, namely that the waves have the correct orientation so that mutual growth of the interfaces occurs. By Eq. (27), this is due to the upwards component of $\tilde{w}$ in the crests of $\tilde{\eta}$ at each of the upper and lower interfaces.

Since the upper and lower vorticity waves have equal phase speeds at $k = 0.5$ (Fig. 7(*a*)) when in isolation, one might be tempted to conclude that this should also be the k of maximum growth. It is true that at $k = 0.5$ the phase difference of the waves is exactly optimal for growth, with $\Delta\theta = \pi/2$, and this results because there is no component of $\tilde{w}$ that is needed to adjust the waves phase speeds (see Eqs. (27) and (28)). However, at this k,

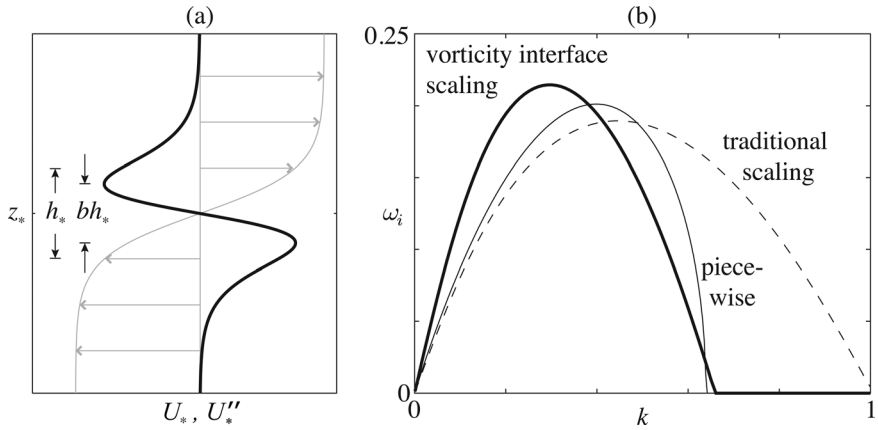

Fig. 8 (*a*) The smooth 'tanh' shear layer velocity profile $U_*(z_*)$ (gray) and the associated vorticity gradient distribution $U_*''(z_*)$ (black). (*b*) Comparison between the growth rates of the smooth tanh-profile and the piecewise linear profile. Growth rates for both the traditional scaling of $U_*(z_*)$ (dashed line) and the vorticity interface scaling (thick solid line) are shown, along with the piecewise result (thin line) for comparison.

the vertical decay of $\tilde{w}$ from each of the waves is still large. The increase in ω_i with decreasing k results from larger amplitudes of the $\tilde{w}$-fields, i.e., A_w in Eq. (27). The k of maximum growth therefore results from a competition between both the changing phase difference of the waves ($\Delta\theta$) required to keep the phase-locked propagation speeds, and the decay of the $\tilde{w}$-fields which controls the relative amplitudes (A_w/A_η) of the waves.

Smooth Shear Layers. The analysis of the piecewise shear layer represents the simplest example that can be used to demonstrate both the wave interaction interpretation, as well as the basic instability of the shear layer. The piecewise $U(z)$ profile is highly idealized, and does not resemble a typical shear layer that would be found in nature; the abrupt 'kinks' in the profile would be smoothed by the action of viscosity. For this reason, the shear layer is often represented by the 'tanh'-profile given in dimensional units by

$$U_*(z_*) = \frac{\Delta U_*}{2}\tanh\left(\frac{2z_*}{h_*}\right) \tag{33}$$

and shown in Fig. 8(*a*). Rather than the δ-function vorticity gradient distribution at the interfaces of the piecewise profile, we now have a smoothly varying $U_*''(z_*)$ that exhibits two peaks at $z_* = \pm bh_*/2$, where $b = 0.6566$, separated by an inflection point at $z_* = 0$ (Fig. 8(*a*)). These peaks in U_*'' can be thought of as two diffuse vorticity interfaces of opposite sign that are interacting in a similar manner as the concentrated interfaces of the piecewise profile.

Analytical solution of the TG equation for this $U_*(z_*)$ presents considerable difficulties, and must be carried out numerically (see, e.g., Refs. [25,26]). The resulting dispersion relation is shown in Fig. 8(*b*) in terms of the dimensionless growth rate $\omega_i = \omega_i^* h_*/\Delta U_*$ (dashed line). This is the traditional scaling for the problem, where the length scale $h_*/2$, and velocity scale $\Delta U_*/2$, have been chosen. It results in the algebraically convenient expression $U(z) = \tanh(z)$ for the dimensionless profile.

Similar to the piecewise profile, the traditional scaling of the tanh shear layer is unstable to long waves that have wavenumbers below some upper cutoff, k_c. Note that the value of $k_c = 1.0$ found for the tanh-profile does not compare exceptionally well to the piecewise result of $k_c = 0.64$. However, recognizing that the relevant length scale for the interaction of the vorticity waves is given by the distance between the interfaces, as in the piecewise profile, we propose that this scale is used for the nondimensionalization of $U_*(z_*)$. Therefore, if we take the length scale of the smooth profile to be given by half the distance between the extrema in the vorticity gradient (U_*''), and the velocity scale to be given by half the velocity difference between these two locations, we then arrive at a dimensionless $U(z)$ of the form

$$U(z) = a^{-1}\tanh(bz) \tag{34}$$

Where $a = \tanh(b)$. The resulting ω_i and k_c, are now very close to the piecewise results (Fig. 8(*b*), 'vorticity interface scaling'). This suggests that the piecewise profiles, though highly idealized, are sufficient to capture the essential instability mechanisms that are present in the more realistic smooth profiles. Further evidence for wave interactions in smooth profiles is discussed in Refs. [15,23,27–30], and also in Sec. 5.

4.2 Stable Interaction: Rayleigh and Fjørtoft Conditions.

The shear layer example above shows how an unstable interaction can occur between vorticity waves when both of the conditions (I, II) are satisfied. It is now demonstrated why each of these conditions is necessary, which will lead to a physical interpretation of the well-known Rayleigh and Fjørtoft stability theorems in terms of wave interactions.

Rayleigh's Theorem. The shear layer is just one example of a flow that exhibits instability due to the presence of an inflection point in the $U(z)$ profile. We saw from the analysis of the tanh-profile that the inflection point separated two regions of oppositely signed vorticity gradients, which can be interpreted as diffuse vorticity interfaces. This is just one of a number of possible profiles that demonstrates Rayleigh's [22] inflection point theorem, which applies to any continuous $U(z)$ profile (i.e., piecewise or smooth), and can be stated as follows.

> Rayleigh's inflection point theorem: A necessary condition for instability is that U'' switch sign somewhere within the domain of flow.

Notice that it is only a necessary condition for instability, and so is useful for quickly judging whether a given profile *may* be unstable; it says nothing about whether a profile *is* unstable. An equivalent theorem for piecewise-linear $U(z)$ is that a necessary condition for instability is that two vorticity interfaces must be of opposite signed ΔQ.

To gain an understanding of why this is the case, we examine a general $U(z)$ profile consisting of two vorticity interfaces at $z = \pm 1$ with the following form (see Fig. 9):

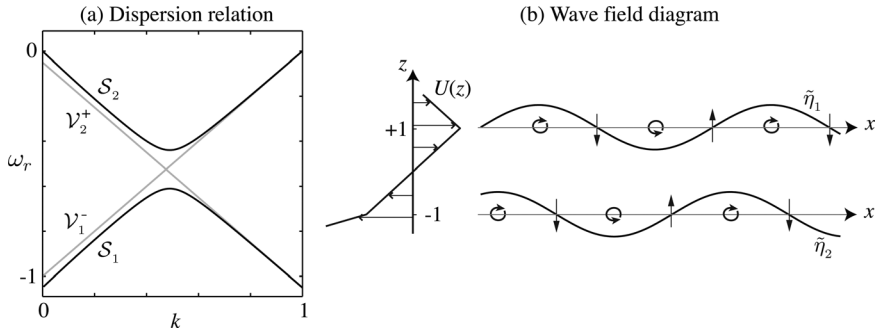

Fig. 9 (*a*) Dispersion relation $\omega_r(k)$ for two stable interacting vorticity waves used to illustrate the Rayleigh inflection point condition. As in Fig. 2 the gray lines indicate the dispersion of waves in isolation from each other. (*b*) Wave field diagram showing that it is not possible for the waves to cause mutual growth in one another—regardless of the relative phase difference. Here an arbitrary phase difference has been chosen for illustration purposes.

$$U(z) = \begin{cases} Q_1(z-1)+1, & z \geqslant 1 \\ z, & |z| \leqslant 1 \\ Q_2(z+1)-1, & z \leqslant -1 \end{cases} \tag{35a}$$

$$Q(z) = \begin{cases} Q_1, & z > 1 \\ 1, & |z| < 1 \\ Q_2, & z < -1 \end{cases} \tag{35b}$$

Note that the piecewise shear layer can be obtained as a special case by setting $Q_1 = Q_2 = 0$. The vorticity jumps across the upper and lower interfaces (1 and 2 subscript, respectively) are given by $\Delta Q_1 = [\![U']\!]_{z_1} = Q_1 - 1$ and $\Delta Q_2 = [\![U']\!]_{z_2} = 1 - Q_2$. The dispersion relation is obtained in the same way as with the piecewise shear layer, and is found to be a quadratic equation in c given by

$$c^2 + a_1 c + a_0 = 0 \tag{36}$$

where

$$a_1 = \frac{-(\Delta Q_1 + \Delta Q_2)}{2k}$$

$$a_0 = \frac{-4k^2 + 2k(\Delta Q_2 - \Delta Q_1) + (1 - e^{-2k})\Delta Q_1 \Delta Q_2}{4k^2}$$

We now examine the particular case, sketched in Fig. 9(*b*), where $Q_1 = -1$ and $Q_2 = 1.1$, so that the vorticity jumps are of the same sign. This means that the vorticity waves present in the profile both have the same (leftward) direction of intrinsic propagation. We will see that this is responsible for violating condition (II) and producing a stable interaction, in keeping with Rayleigh's inflection point theorem.

It is easily verified using Eq. (25) that the isolated vorticity wave speeds are equal for $k = 0.48$, which can be seen in the crossing of $\mathcal{V}_1^-$ and $\mathcal{V}_2^-$ in the dispersion relation shown in Fig. 9(*a*). However, unlike Rayleigh's shear layer, there is no k for which unstable modes are found. The only sign of interaction between the vorticity waves in this case are the relatively small departures of the stable wave modes $\mathcal{S}_1$ and $\mathcal{S}_2$ from the dispersion curves of the isolated waves $\mathcal{V}_1^-$ and $\mathcal{V}_2^-$. Near the point $k = 0.48$ where $\mathcal{V}_1^-$ and $\mathcal{V}_2^-$ meet, the modes $\mathcal{S}_1$ and $\mathcal{S}_2$ appear to switch identity and follow the isolated dispersion relations of the other modes more closely. We shall not discuss this behavior in detail, but refer the interested reader to Craik [31]. The fact that no instability occurs in this case is due to the waves having an orientation that is incapable of achieving mutual growth, i.e., a violation of condition (II). Once again, the wave-field diagram demonstrates visually why this is so, and is shown in Fig. 9(*b*).

By inspection of Fig. 9(*b*), it can be seen that no matter the phase difference between the upper and lower vorticity waves, it is not possible for *both* waves to grow simultaneously. This is due to the relationship between $\tilde{w}$ and $\tilde{\eta}$ in each of the waves, which is determined entirely by their direction of intrinsic propagation. If one of the waves were to have a rightward intrinsic propagation, it would be equivalent to reversing the direction of $\tilde{w}$ or taking the mirror image of $\tilde{\eta}$ in a horizontal axis, which can then be seen to be capable of producing a mutual growth of both interfaces. We can therefore conclude that it is necessary to have two vorticity waves with an *opposite intrinsic propagation* in order for instability to be possible, and that this is fulfilled if the vorticity jumps are of opposite sign, i.e., if an inflection point is present. This provides a physical interpretation of Rayleigh's inflection point theorem in terms of wave interactions. Cairns [32] discusses an equivalent argument of this principle in terms of wave energy.

Fjørtoft's Extension. Seventy years after Rayleigh's inflection point theorem was published, it was extended by Fjørtoft [33].

> Fjørtoft's extension: A necessary condition for instability is that $U''(U - U_s) < 0$ somewhere within the domain of flow, where $U''(z_s) = 0$, and $U_s = U(z_s)$ is the velocity at the level of an inflection point.

Again, only a necessary condition on any continuous $U(z)$ profile, Fjørtoft's extension strengthens the Rayleigh inflection point theorem by excluding certain types of inflection points.

Fjørtoft's extension seems, at first sight, to be an abstract and nonintuitive condition for determining the stability properties of a given profile. However, the physical interpretation becomes clear if we look at the specific example from the piecewise profiles of Eq. (35) with $Q_1 = Q_2 = 0.5$. Substituting these values into Eq. (36) leads to the dispersion relation shown in Fig. 10(*a*), where the isolated vorticity wave dispersion curves $\mathcal{V}_1^+$ and $\mathcal{V}_2^-$ are also shown in gray. It can be seen that there is no value of k for which the wave speeds are equal. This is in violation of condition (I), and precludes the possibility of phase-locking, despite the fact that a configuration of mutual growth could, in principle, be achieved.

The inability of the vorticity waves to phase lock as k is varied (and therefore also the wave speed) can be seen to be a general condition described by Fjørtoft's extension: if $U''(U - U_s) > 0$, and so the flow must be stable, the regions of the profile associated with $U'' > 0$, describing vorticity waves with a rightward intrinsic propagation speed, must have an advection by the mean flow relative to the inflection point $(U - U_s)$ with the same sign, and is therefore reinforcing this propagation. The same is true of the leftward-propagating waves on the other side of the inflection point, and thus the wave modes are ensured never to cross in the dispersion relation. Once again, we illustrate this graphically with the wave field diagram in Fig. 10(*b*).

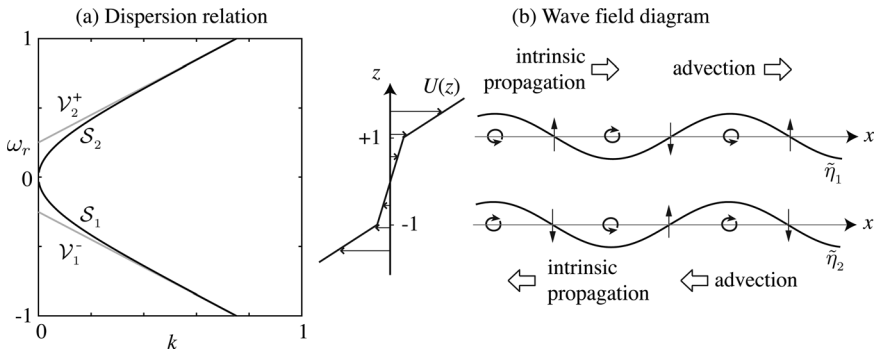

Fig. 10 (*a*) Dispersion relation for two stable vorticity waves that demonstrate Fjørtoft's extension (notation as in Fig. 2). (*b*) Wave field diagram showing the reinforcement of the intrinsic wave propagation by the advection of the mean flow profile that is stable by Fjørtoft's extension.

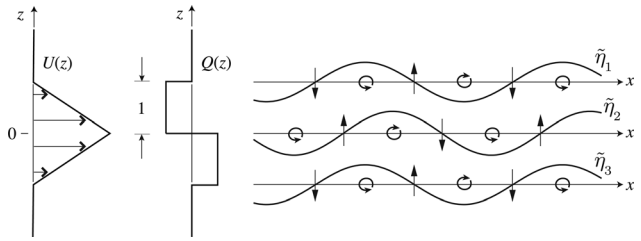

Fig. 11 Profiles of *U*(*z*) and *Q*(*z*) for the triangular jet flow, together with the wave field diagram at $k = 0.5$

Summary. In summary, we have shown that there is a simple physical interpretation of Rayleigh's theorem and Fjørtoft's extension in terms of wave interactions. They can both be understood in terms of the wave interaction conditions I and II from Sec. 3. Rayleigh's inflection point theorem insures that the waves are able to induce *mutual* growth in each other. We found that this is only possible if the vorticity waves have an opposite ΔQ, which means that they are oppositely propagating. Fjørtoft's extension ensures that it is possible for the waves to achieve a phased-locked state. This is done by restricting the profiles such that the mean flow advection and the intrinsic propagation speed of the waves do not reinforce each other.

It is also straightforward to see why these theorems are necessary for instability, but not sufficient; they both describe situations where instability will not be possible, i.e., where one of the conditions I, II, are not satisfied.[3] However, in most situations of interest if both the Rayleigh and Fjørtoft conditions are satisfied the flow is very likely to be unstable.

4.3 The Unstable Modes of a Jet: An Example. Jetlike flows, with a $U(z)$ consisting of a finite region of momentum, naturally arise in many fluid mechanical applications. Similar to the shear layer, it can be considered as a natural building block of turbulent flows. Here we shall briefly apply the results discussed so far to examine the unstable modes of a jet flow.

The background velocity and vorticity profiles that we use are that of the triangular jet (see Drazin [34], Sec. 8.3, and Heifetz et al. [18]), with the piecewise representation shown in Fig. 11. The profile consists of three vorticity interfaces (labeled 1 through 3 starting at the top of the profile), and allows for two interactions between the central interface and each of the vorticity waves on either side. We have chosen the maximum velocity of the jet as our unit of velocity, and the distance between each vorticity interface as our unit of length. It can immediately be seen that the triangular jet satisfies both the Rayleigh and Fjørtoft conditions, and instability is therefore possible.

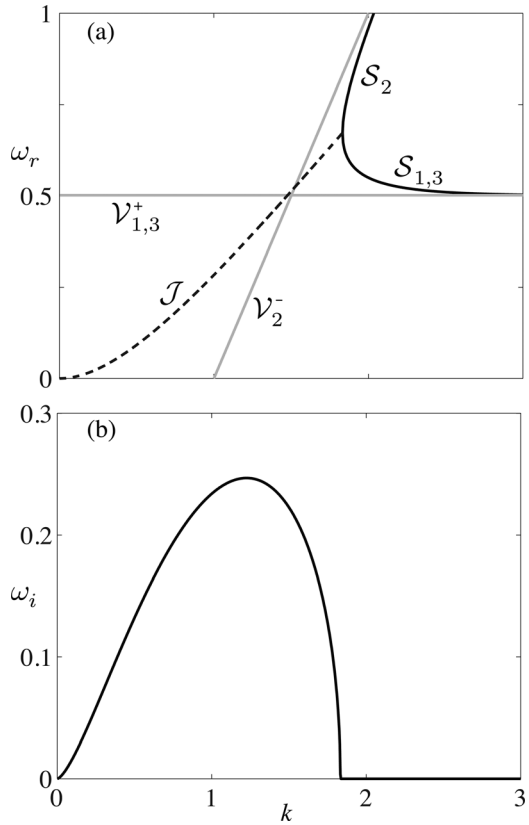

Fig. 12 Dispersion relation for the triangular jet. The frequencies of the isolated vorticity waves (gray curves, $\mathcal{V}_{1,2,3}$), the stable waves (solid curves, $\mathcal{S}_{1,2}$), and the unstable jet mode (dashed curve, $\mathcal{J}$) are shown in (*a*), with the growth rate in (*b*).

The dispersion relation and growth rate curves may be found by the same procedure as in Sec. 4.1, using Eq. (31) at each interface to arrive at a homogeneous system of equations that leads to the dispersion relation. It is possible to factor the cubic dispersion relation into a stable root given by $c = (1 - e^{-2k})/2k$, and the quadratic equation

$$2k^2c^2 + k(1 - 2k - e^{-2k})c - [1 - k - (1 + k)e^{-2k}] = 0 \quad (37)$$

which gives an unstable mode for $0 < k \lesssim 1.83$ as shown in Fig. 12. The unstable mode is often referred to as the sinuous

[3]The Rayleigh and Fjørtoft theorems can also be interpreted in terms of the conservation of pseudomomentum and pseudoenergy, respectively, and the interested reader is referred to Heifetz et al. [11] for further details.

mode, because the displacements of the flanks of the jet (i.e., interfaces 1 and 3) are in phase with each other. The other possible mode of the jet is the varicose mode, consisting of displacements in antiphase on the jet flanks, corresponding to the stable root found above. These two possible modes of the jet are a general property of any flow that is an even function about some line of symmetry ($z=0$ in this case), with symmetric boundary conditions [34].

Due to the symmetry of the unstable sinuous mode, it is possible to visually interpret the wave interactions leading to instability in terms of the wave field diagram (Fig. 11). Because the jet flanks are always in phase with each other, they undergo phase speed modifications, but do not cause any growth rate in each other. The Rayleigh condition requires that the unstable interaction take place between the central interface and the jet flanks. This interaction is essentially the same as the shear layer except it is present on each side of the jet—corresponding to an unstable interaction across the inflection points. As the isolated phase speed of the jet flanks ($\mathcal{V}_{1,3}$ in Fig. 12(*a*)) diverge from the central interface speed ($\mathcal{V}_2$) phase-locking is not possible, and similar to the shear layer, the flow is stabilized.

5 Stratified Shear Flows

When considering the stability of stratified shear flows, one might be tempted to presume that the *statically stable* density field acts as a stabilizing influence on the flow. In doing so, it would suppress the growth of instabilities, and possibly prevent the flow from transitioning to turbulence. Though this is certainly the case in some instances, the statically stable stratification can also act as a *destabilizing* influence; producing instabilities that would otherwise be absent in the same shear flow of a homogeneous fluid. This feature of stratified shear flows, discussed by Howard and Maslowe [35], is just one example of a number of puzzling, yet fundamental, results, that underscores the need to develop a physical interpretation of the mechanisms that operate to produce instability in these flows.

Within the wave interaction interpretation, the source of the destabilizing effect of stable stratification is due to the presence of internal gravity waves, which may interact to produce instability in the same way as two vorticity waves in a homogeneous flow [14,15,17,24,27–30,35]. This leads to the possibility of new types of instabilities, which we now describe.

5.1 The Instabilities of Holmboe and Talyor–Caulfield

The Holmboe Interaction. The first instability resulting from the presence of statically stable density stratification that we shall discuss is the Holmboe (H) instability. It was first recognized and described in terms of wave interactions in the seminal paper of Holmboe [14]. Holmboe was also, to our knowledge, the first to systematically describe shear instability in terms of wave interactions.[4] The H instability results from the interaction between a vorticity wave and an internal gravity wave. This is best seen by the following dimensionless profiles:

$$U(z)=\begin{cases}1, & z\geqslant 1\\ z, & z<1\end{cases}\quad\text{and}\quad \bar{\rho}(z)=\begin{cases}0, & z\leqslant 0\\ 1, & z>0\end{cases}\tag{38}$$

where the dimensionless density profile is defined as $\bar{\rho}\equiv(\bar{\rho}_*-\rho_0^*)/\Delta\rho_*$. These profiles were first analyzed by Baines and Mitsudera [15].

Once again we have an eigenfunction describing the interaction of two interfacial waves given by

$$\hat{\psi}(z)=Ae^{-k|z-1|}+Be^{-k|z|}\tag{39}$$

and a dimensionless jump condition that allows for density stratification given by

$$\left[\!\left[(U-c)\hat{\psi}'-U'\hat{\psi}\right]\!\right]_{z_i}+\frac{J}{U_i-c}\hat{\psi}_i=0\tag{40}$$

where $J\equiv g'_*L_*/V_*^2$ is a dimensionless measure of the strength of the stratification at the density interface versus the shear, and is referred to as a bulk Richardson number. Recall that L_* and V_* are the length and velocity scales that are chosen for the nondimensionalization. The resulting dimensionless profiles are shown in Fig. 13(*a*).

The stability properties of the dispersion relation are shown on the stability diagram of Fig. 13(*c*). In the homogeneous case, at $J=0$, the flow is stable and consists of a single vorticity wave. However, once $J>0$ instability can be seen to be focused in a strip in the kJ-plane (white region contoured with ω_i in Fig. 13(*c*)) that extends to large J and k, and reaches its maximum growth rate at a finite value of J. The otherwise stable density stratification has destabilized the flow.

The location of the unstable strip in the kJ-plane can be approximated by consideration of the wave interactions that are expected to lead to instability [15,17,36]. For example, in the present profiles, from condition (II), we expect that instability will result from the interaction of the leftward-propagating vorticity wave and the rightward-propagating gravity wave ($\mathcal{V}^-$ and $\mathcal{G}^+$ in Fig. 13(*d*), respectively). This can also be seen directly from the dispersion relation $\omega_r(k)$ shown in Fig. 13(*d*), taken at a value of $J=2$. Since, by condition (I), these waves must phase-lock to become unstable, the region of instability should be centered close to the 'resonance' condition

$$\mathcal{V}_1^-\leftrightarrow\mathcal{G}_2^+\quad\Rightarrow\quad J=2k\left(1-\frac{1}{2k}\right)^2\tag{41}$$

This resonance condition is merely the point at which the isolated waves cross in the dispersion diagram, and describes a curve in the kJ-plane (Eq. (41), and dot-dashed line in Fig. 13(*c*)). It is approximate since it does not account for any interaction between the waves, which can alter the region where phase-locking occurs. However, the accuracy of this resonance condition improves with increasing k since the interaction between the interfaces decays exponentially with k. This can be seen in the stability diagram of Fig. 13(*c*) as the unstable region narrows around the resonance condition as k increases.

The H instability can be viewed on a wave field diagram, similar to the homogeneous shear flows of the previous section (Fig. 13(*b*)). In the unstable band of k the rightward propagating internal wave and the vorticity wave have achieved a phase-locked state. Figure 13(*b*) shows that a Rayleigh-type condition is also satisfied where the two interfaces have the correct $\tilde{\eta}$ and $\tilde{w}$ relationship to cause mutual growth. Recall that for an internal gravity wave, the $\tilde{q}$ field has a variable phase relationship with its own $\tilde{\eta}$ field. This is not the case in Fig. 13(*b*) because we have plotted the wave fields directly on the resonance condition. This aspect of stratified shear flows complicates the analysis, however, the gravity wave kernel technique [28,29] can be used to simplify the analysis, and this is discussed below.

It is instructive to examine the case in which the density interface is located in the region of zero shear above the vorticity interface, i.e., the profiles given by

$$U(z)=\begin{cases}0, & z\geqslant 0\\ z, & z<0\end{cases}\quad\text{and}\quad \bar{\rho}(z)=\begin{cases}0, & z\leqslant 1\\ 1, & z<1\end{cases}\tag{42}$$

and illustrated in Fig. 14(*a*). The important difference between these profiles and those of Fig. 13 is that the interfaces now have the same advective velocity, which we take as zero for simplicity. There are now no unstable modes present. The only possible

[4]Although the work of Garcia [23] was published 6 years previous to Holmboe's [14] paper, Garcia directly acknowledges Holmboe with the wave interaction concept in an acknowledgments section that appears (unusually) in the main body of the paper.

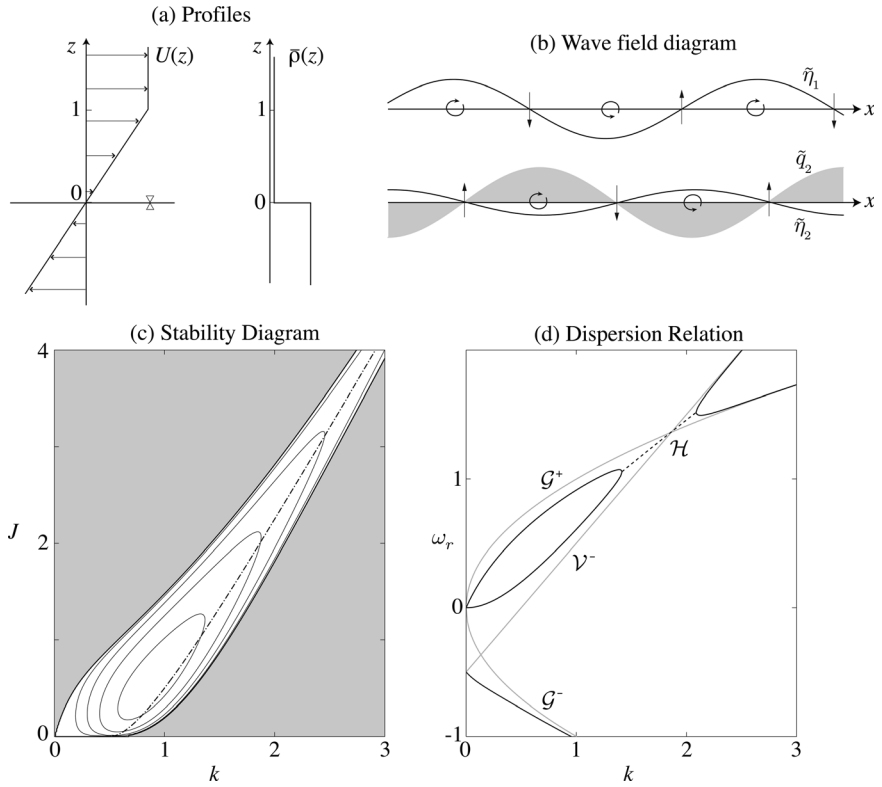

Fig. 13 (*a*) Profiles of $U(z)$ and $\bar{\rho}(z)$ that demonstrate the unstable Holmboe interaction between a vorticity wave (at $z=1$) and an internal gravity wave (located at $z=0$). (*b*) The wave field diagram showing the structure of the unstable mode with $J=2$, $k=1.87$. The gray shading is used to indicate the $\tilde{q}_2$ field, which may have a phase difference from the $\tilde{\eta}_2$ field. (*c*) Stability diagram showing the Holmboe unstable region. Contours are of growth rate (ω_i) with an interval of 0.03, and the thick solid lines indicate the stability boundary with stable regions in gray. The resonance condition is denoted by the dot-dashed line and follows very closely the unstable region. An example of the dispersion relation $\omega_r(k)$ shown in (*d*) is taken at $J=2$.

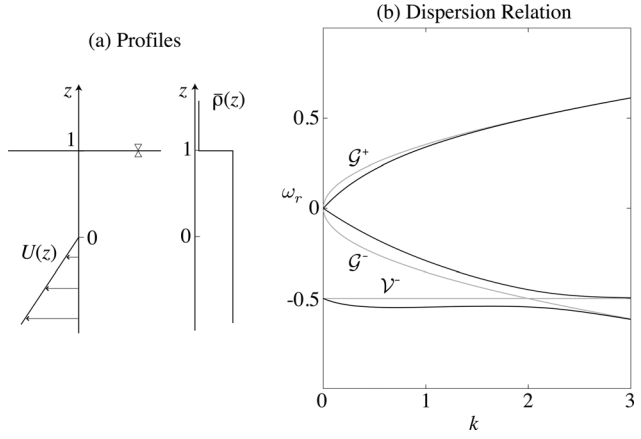

Fig. 14 (*a*) Profiles that demonstrate a stable interaction between a gravity wave and a vorticity wave. An example of the dispersion relation $\omega_r(k)$ is shown in (*b*) for $J=0.25$. See Fig. 2 for further notation.

unstable interaction is between the oppositely propagating waves $\mathcal{G}^+$ and $\mathcal{V}^-$, which is stable by a Fjørtoft-type condition; they are unable to phase-lock, as is required for condition (I). This can be seen in the dispersion relation in Fig. 14(*b*) since their phase speeds are unable to cross. Similarly, the $\mathcal{G}^- \leftrightarrow \mathcal{V}^-$ interaction must be a stable one, by a Rayleigh-type condition; they have the same direction of intrinsic propagation and therefore cannot achieve a state of mutual growth, as required for condition (II). As in the stable interaction of two vorticity waves (Fig. 9), the stable modes appear to switch identity near what would be their crossing if they were in isolation. This example emphasizes the similarity between the conditions governing wave interactions in homogeneous flows and stratified flows.[5]

The Taylor–Caulfield Interaction. Just as the H-instability may result from the interaction of a vorticity and a gravity wave, so too may an instability occur between two gravity waves. The quintessential profiles for examining this instability are those shown in Fig. 15(*a*), and were first studied by Taylor [38]. In his 1931 paper, Taylor was perhaps the first to recognize the connection between the region of instability in the kJ-plane and the matching of the phase speeds of the isolated interfacial waves. Taylor [38] states: "the instability [at large k] may therefore be regarded as being due to a backward-moving free wave at the upper surface of separation forcing a forward-moving free wave at the lower surface of separation when the velocity in space of the two waves coincides." However, little else on this remarkable observation was mentioned in the rest of the paper, and it was not until many decades later that the consequences of this interpretation were fully appreciated. Caulfield [17] demonstrated the wave interactions occurring in a similar, though slightly more complicated, profile that also included two vorticity interfaces. He was also the

[5]The stability of this particular flow may also be interpreted in terms of an energetics perspective. The stable flow is due to the lack of a shear growth source—the waves must either be embedded within the shear or at its sides in order to be able to extract energy from it. See Harnik and Heifetz [37] and Rabinovich et al. [29] for further details.

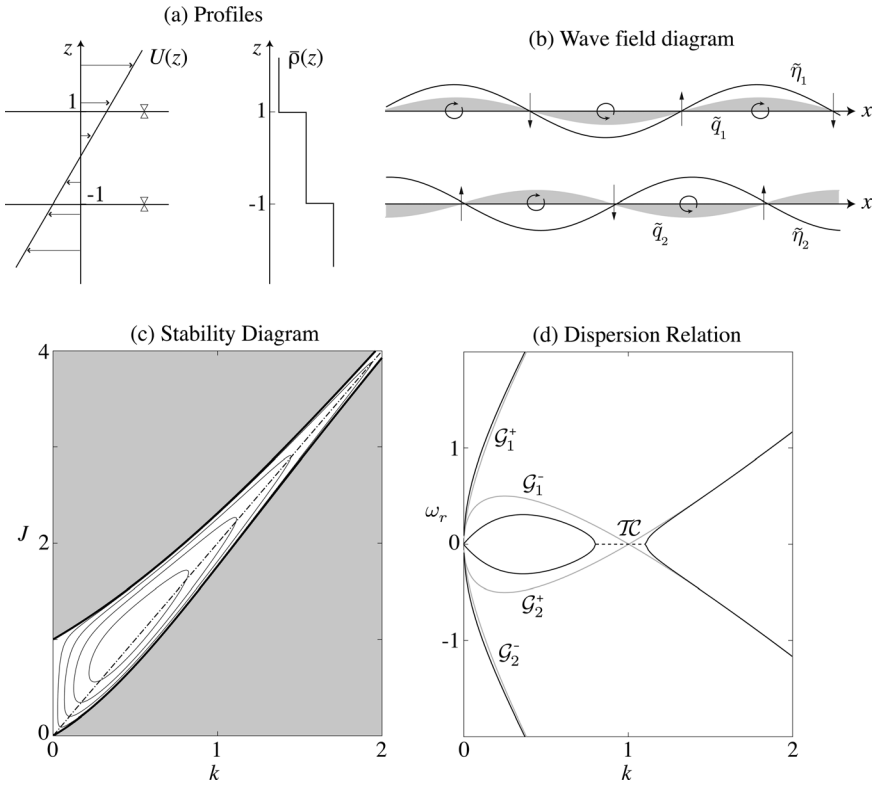

Fig. 15 (*a*) Dimensionless profile of background velocity $U(z)$ that demonstrates the unstable Taylor–Caulfield interaction between two internal gravity waves (at $z = \pm 1$). (*b*) The wave field diagram showing the structure of the unstable mode with $J = 2$, $k = 1$. (*c*) Stability diagram showing the Taylor–Caulfield unstable region (see Fig. 13(*c*) for notation). An example of the dispersion relation $\omega_r(k)$ shown in (*d*) is taken at $J = 2$.

first to use these interactions as a general classification of the different types of unstable modes (see also Ref. [39]).

As with the analysis of the Holmboe interaction, we may find the dispersion relation, and plot the stability diagram (Fig. 15(*c*)) by applying Eq. (40) at each density interface. Again, the unstable region is located in a strip that is centered on the resonance condition at large k. This is given by equating the phase speeds of the leftward-propagating gravity wave on the upper interface with the rightward-propagating gravity wave on the lower interface, i.e.,

$$\mathcal{G}_1^- \leftrightarrow \mathcal{G}_2^+ \quad \Rightarrow \quad J = 2k \tag{43}$$

assuming each interface has an equal g'_*. This unstable interaction is the only one that is possible in these profiles since the $\mathcal{G}_1^+ \leftrightarrow \mathcal{G}_2^-$ interaction is stable by a Fjørtoft-type argument; advection by the background profile reinforces the phase speed differences to ensure that the modes never cross in the dispersion relation (see Fig. 15(*d*)).

5.2 The Use of Gravity Wave Kernels. No major differences are present between the wave interaction approach in homogeneous and stratified shear flows, and the unstable interactions between waves may still be viewed on a wave field diagram, as shown in Fig. 13(*b*). However, the analysis does become slightly more complicated in the case of stratified flows because a phase shift may occur between the $\tilde{\eta}$ and $\tilde{q}$ fields in the gravity wave. Whereas the vorticity wave always has a phase shift of 0 or 180 deg (depending on the sign of ΔQ), since $\tilde{q}$ is directly tied to $\tilde{\eta}$ through Eq. (13), the gravity wave has a variable phase difference. This is because the baroclinic $\tilde{q}$ must be expressed in terms of the *generation* of $\tilde{q}$, i.e., a rate of change as in Eq. (16).

In order to simplify the wave interactions between gravity waves, and to draw a direct analogy with vorticity waves, Harnik et al. [28] have defined so-called wave kernels. This approach consists of deconstructing the displacement and vertical velocity fields into components that have a phase shift of 90 deg (see Figs. 3 and 4), thus allowing any density interface $\tilde{q}$ and $\tilde{\eta}$ to be represented in terms of two superimposed stable waves. This approach uses the kernels as building blocks for constructing the wave interactions solely in terms of stable waves.

In particular, for a given normal mode, we can define $\tilde{\eta}$ and $\tilde{q}$ at any interface (either vorticity, density, or both) as

$$\tilde{\eta} \equiv \tilde{\eta}^+ + \tilde{\eta}^- \quad \text{and} \quad \tilde{q} \equiv \tilde{q}^+ + \tilde{q}^- \tag{44}$$

In order to satisfy the requirement that each component be associated with a stable interfacial wave, we must specify the relationship between $\tilde{\eta}^\pm$ and $\tilde{q}^\pm$. This is done through the kinematic condition (Eq. (18)), which can be written as

$$(U - c)\hat{\eta} = -\hat{\psi} \tag{45}$$

assuming a normal mode form. To relate $\hat{\psi}$ to the normal mode vorticity $\hat{q}$, we use the definition

$$\hat{\psi}'' - k^2\hat{\psi} = \hat{q} \tag{46}$$

Since we are dealing with an interface with a δ function distribution of vorticity, we write $\hat{q} = \tilde{q}_\ell \delta(z - z_\ell)$, and use the solution for $\hat{\psi}(z)$ found in Eq. (22) to show $\tilde{q}_\ell = -2k\psi_\ell$, after integrating across the interface and taking the stream function amplitude at

the interface as ψ_ℓ. The relationship between $\tilde{q}_\ell$ and $\tilde{\eta}_\ell$ at the interface is now clear, and can be written as in Harnik et al. [28] (except for a minus sign due to a different definition of $\tilde{q}$) as $\tilde{q}_\ell = 2k(U-c)\tilde{\eta}_\ell$. Note again, as in Sec. 2.3, that we are being loose with our notation and $\tilde{q}_\ell$ is really the strength of the circulation per wavelength, and not precisely the vorticity.

The final step in defining the wave kernel is to force the $\tilde{q}-\tilde{\eta}$ structure to satisfy the dispersion relation of the interface, assuming that it is in isolation, i.e., no interaction. This can be done using Eq. (24) to define $c^{\pm}_{\ell *}$ in dimensional units by

$$U^*_\ell - c^{\pm}_{\ell *} = -\frac{\Delta Q_*}{4k_*} \pm \left[\left(\frac{\Delta Q_*}{4k_*}\right)^2 + \frac{g'_*}{2k_*}\right]^{1/2} \tag{47}$$

The wave kernels are then given by

$$\tilde{q}^{\pm}_\ell = 2k(U_\ell - c^{\pm}_\ell)\tilde{\eta}^{\pm}_\ell \tag{48}$$

Since the $c^{\pm}_\ell$ must be real numbers, this ensures that each kernel is a stable wave solution of the isolated dispersion relation, and that each has a $\tilde{q}_\ell$ and $\tilde{\eta}_\ell$ that is either in or out of phase with each other.

5.3 Mixed Modes and Smooth Profiles. Thus far, we have limited our discussion of the wave interaction interpretation primarily to profiles that exhibit only a single dominant unstable interaction when the conditions (I,II) are satisfied. However, it is often the case that there may be multiple unstable interactions that are possible, and distinguishing the various types is not always a straightforward task. A general classification of the unstable interactions in stratified shear flows was presented in Refs. [17,27] in terms of three fundamental mechanisms: (i) the Kelvin–Helmholtz (KH) interaction of two vorticity waves,[6] (ii) the Holmboe (H) interaction of an internal gravity wave and a vorticity wave, and (iii) the Taylor–Caulfield (TC) interaction of two internal gravity waves. It is perhaps most instructive to introduce multiple interactions with an example.

Holmboe's Stratified Shear Layer. Consider a general stratified shear layer similar to that analyzed in Holmboe's [14] original paper. The dimensionless piecewise profiles are given by

$$U(z) = \begin{cases} 1, & z > 1 \\ z, & |z| \le 1 \\ -1, & z < -1 \end{cases} \quad \text{and} \quad \bar{\rho}(z) = \begin{cases} 0, & z \geqslant -\varepsilon \\ 1, & z < -\varepsilon \end{cases} \tag{49}$$

with the density interface located some dimensionless distance ε, below the center of the shear layer. This flow can be set up in the laboratory by injecting a lighter fluid above a heavier fluid [42]. These profiles exhibit two vorticity interfaces at $z = \pm 1$, and a density interface at $z = -\varepsilon$, that admit a total of four wave modes, i.e., two gravity modes $\mathcal{G}^{\pm}$ and two vorticity modes $\mathcal{V}^{\pm}$. There are two different types of interactions that are possible: the $\mathcal{V}^{+} \leftrightarrow \mathcal{V}^{-}$ interaction, that is commonly referred to as KH, and the H interactions between $\mathcal{G}^{\pm} \leftrightarrow \mathcal{V}^{\mp}$. The stability diagram for these profiles is shown in Fig. 16, and, in the case of symmetric profiles with $\varepsilon = 0$ (Figs. 16(*a*) and 16(*b*)), can be seen to exhibit two relatively distinct regions of instability: (i) the region of stationary instability that exists for relatively low J, and (ii) the region of propagating modes (thin gray contours) that extends to large J. These regions have traditionally been associated with the stationary KH instability at low J, and the propagating H instability at high J,

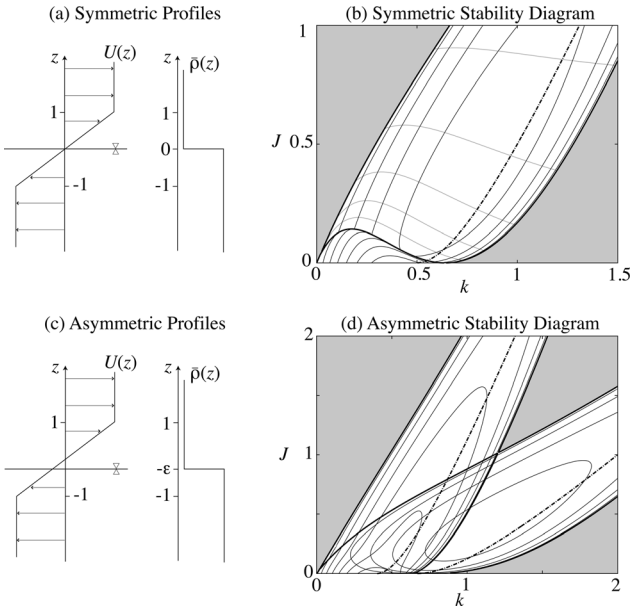

Fig. 16 (*a*) Profiles for Holmboe's [14] symmetric ($\varepsilon = 0$) stratified shear layer. (*b*) The associated symmetric stability diagram where the gray area represents stable regions, with the thick dark line denoting the stability boundary, as well as the transition from propagating to stationary modes. The thin dark lines are contours of growth rate, ω_i, with spacing of 0.03, and the thin gray contours represent the phase speed c_r, with spacing 0.2. (*c*), (*d*) Profiles and stability diagram for the asymmetric stratified shear layer with $\varepsilon = 0.25$. In both (*b*), (*d*) the dashed-dotted line represents the resonance condition between vorticity and gravity waves.

and they can be seen to represent the competition of these two distinct interactions.

The transition between stationary and propagating instabilities can be understood by starting with the homogeneous Rayleigh instability at $J = 0$. In this limiting case the vorticity waves are in a phase-locked state with a stationary phase speed (see Sec. 4.1). As J increases, the amplitude of the vertical velocity field increases, and so does the intrinsic propagation speed of the isolated gravity waves on the density interface. Eventually, a critical value of J must be reached where the vorticity waves are no longer able to prevent the propagation of the gravity waves; the unstable modes must propagate at sufficiently high J.

Although the transition between stationary and propagating unstable modes in Fig. 16(*b*) is abrupt—and coincides with a (continuous) change in the growth rate behavior—it is misleading to assume that this also indicates an abrupt switch from a purely KH- to an H-type interaction. In fact, the KH interaction can be shown to exist in the region of propagating modes that are normally considered of the H-type [27]. This intermingling of the two different interactions for a given unstable mode, which we shall refer to as a *mixed mode*, becomes more obvious if we modify Holmboe's profiles to include a shift between the center of the shear layer and the density interface.

Keeping the velocity profile unchanged, we lower the density interface to the dimensionless level $z = -\varepsilon$. This breaks the symmetry of the profiles and results in two branches of instability, as can be seen in Fig. 16(*d*) for $\varepsilon = 0.25$. At large k these branches fall on the resonance condition for the two possible H-type interactions, i.e., $\mathcal{V}^{-}_1 \leftrightarrow \mathcal{G}^{+}$ and $\mathcal{V}^{+}_2 \leftrightarrow \mathcal{G}^{-}$, shown with the dot-dashed lines. However, as J is reduced we must have a diminishing strength of the density interface on the unstable interactions, until $J = 0$ when the homogeneous shear layer is recovered and instability is purely KH. This indicates that there is a transition from the KH to the H interaction as J is increased. This transition is gradual

[6] It is more appropriate to refer to this vorticity-vorticity wave interaction as the Rayleigh [22] mechanism, however, it has become conventional in the stratified shear flow literature to use KH after Kelvin [40] and Helmholtz [41], and we shall stick with this notation in the remainder of the paper.

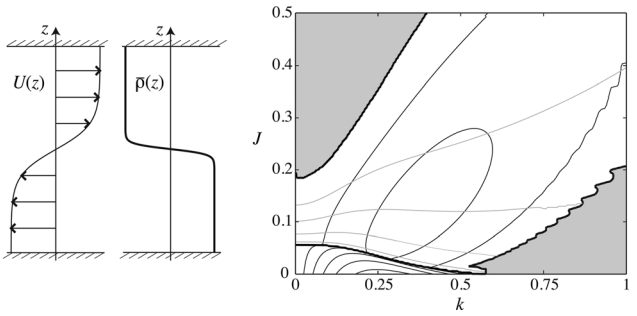

Fig. 17 Profiles and stability diagram for the smooth profiles of Holmboe's [14] symmetric ($\varepsilon = 0$) stratified shear layer with $R = 5$. All notation the same as in Fig. 16. Oscillations appear on the high-k stability boundary due to issues in numerical resolution (see Ref. [43] for more details).

and is generally composed of a mix of both types of interactions [27].

This example demonstrates that instability in profiles with multiple interfaces generally involves multiple interactions, and these interactions can take place simultaneously in the same unstable mode.

Smooth Profiles. In Sec. 4.1, we examined the smooth 'tanh' shear layer, and argued that the relevant scaling in terms of the KH vorticity wave interactions leads to the dimensionless velocity profile

$$U(z) = \frac{1}{a}\tanh(bz) \tag{50}$$

The high wavenumber cutoff for instability, as well as the growth rate curve ($\omega_i(k)$), was similar to that found in the piecewise representation of $U(z)$. If we now combine the profile of Eq. (50) with the following density profile:

$$\bar{\rho}(z) = -\frac{1}{2}\tanh(bRz) \tag{51}$$

we can assess the stability of a smooth (symmetric) stratified shear layer. The dimensionless parameter R is defined as the ratio of the shear layer thickness to the thickness of the density interface, and if we take R to be large we approach a flow that is similar to Holmboe's symmetric shear layer, with a density interface much thinner than the shear layer thickness.

Analytical solutions to the TG equation for the profiles in Eqs. (50) and (51) are difficult, and a numerical solution is usually employed [13,26,43]. The resulting stability diagram, for $R = 5$, is shown in Fig. 17. It is strikingly similar to the stability diagram obtained for piecewise profiles (Fig. 16(*a*)). Again, it consists of two distinct regions of unstable modes: stationary modes at low J, and propagating modes at larger J. As R is increased, the growth rate of the propagating modes increases [43,44], and the piecewise and smooth diagrams become more similar. The similarity is an indication that the same wave interaction mechanisms are acting in the smooth profiles as in the piecewise profiles.

This interpretation can be further developed by considering first the homogeneous ($J = 0$) shear layer from Sec. 4.1. In the piecewise representation, the two vorticity waves, located where U'' has δ function behavior, interact to produce instability. However, in the smooth 'tanh' shear layer, U'' is distributed in two 'interfacial regions' that have extrema at $z_* = \pm bh_*/2$, in dimensional units (see Fig. 8). Just as with the piecewise vorticity interface, once the smooth interfacial region is perturbed by a (sinusoidal in x) vertical displacement $\hat{\eta}(z)$, it will produce a perturbation velocity field that can interact with the second interfacial region across the inflection point.

Mathematically, this can be seen from the TG equation for a homogeneous shear flow (referred to as Rayleigh's equation)

$$\hat{\psi}'' - k^2\hat{\psi} = -U''\hat{\eta} \tag{52}$$

with the normal mode form of the linearized kinematic condition, i.e., $\hat{\eta} = -\hat{\psi}/(U - c)$, used on the rhs. This equation expresses the perturbation vorticity (l.h.s.) in terms of the vertical displacement of the background vorticity gradient (rhs). To solve for $\hat{\psi}$, we use the Green's function approach and write

$$\hat{\psi}(z) = -\int_D G(s,z)U''(s)\hat{\eta}(s)ds \tag{53}$$

where D denotes the vertical domain of the problem, and $G(s,z)$ is the appropriate Green's function, which in the case of an unbounded domain is given by

$$G(s,z) = -\frac{1}{2k}e^{-k|s-z|} \tag{54}$$

Equation (53) shows that a smooth interfacial vorticity region may be treated as a continuous superposition of piecewise vorticity interfaces, each of strength $-U''\hat{\eta}$. The piecewise results discussed earlier can be seen to be a special case that are recovered from Eq. (54) by substituting $U''(z) = \Delta Q\delta(z - z_\ell)$.

This Green's function approach has been used to study wave interactions in stratified shear flows with smooth profiles [27,28]. Carpenter et al. [27] describe a method whereby the perturbation velocity field, described by ψ, is split into a kinematic component associated with the vorticity interface regions of the shear layer ψ_K, and a baroclinic component that arises from the density interface regions, ψ_B (see Sec. 2.2). Using the Green's function approach these two distinct fields may be extracted from the normal modes using

$$\hat{\psi}_K(z) = -\int_{D_K} G(s,z)U''(s)\hat{\eta}(s)ds \tag{55}$$

and,

$$\hat{\psi}_B(z) = \int_{D_B} G(s,z)\frac{N^2(s)}{U(s) - c}\hat{\eta}(s)ds \tag{56}$$

where the integrations are carried out over the vorticity D_K, and density D_B, interfacial regions. These relationships can then be used to construct the vertical velocity fields from distinct interfacial regions: vorticity regions using $\hat{\psi}_K$, and density regions using $\hat{\psi}_B$.

A problem arises when we wish to determine whether this vertical velocity field is causing growth or propagation of some other distant interface. This is due to the fact that we no longer have a single displacement, but instead a continuous displacement $\hat{\eta}(z)$ over the interfacial *region*. This raises the question: how do we calculate a growth or a phase speed contribution that describes the interaction in this case? This is an essential difficulty in the extension of wave interactions to smooth profiles. One strategy used by Carpenter et al. [27] is to use an integrated measure across the whole interfacial region with the $U''(z)$ and $N^2(z)$ profiles as weight functions. This is a natural choice since the piecewise result is recovered; however, there is still a degree of arbitrariness to the procedure. Nonetheless, the result of this approach is an equivalent interpretation of wave interactions in smooth profiles in which the results have been found to agree well with those of the piecewise profiles [27].

5.4 An Example of Geophysical Shear Flow Instability. A great advantage of extending the wave interaction analysis to

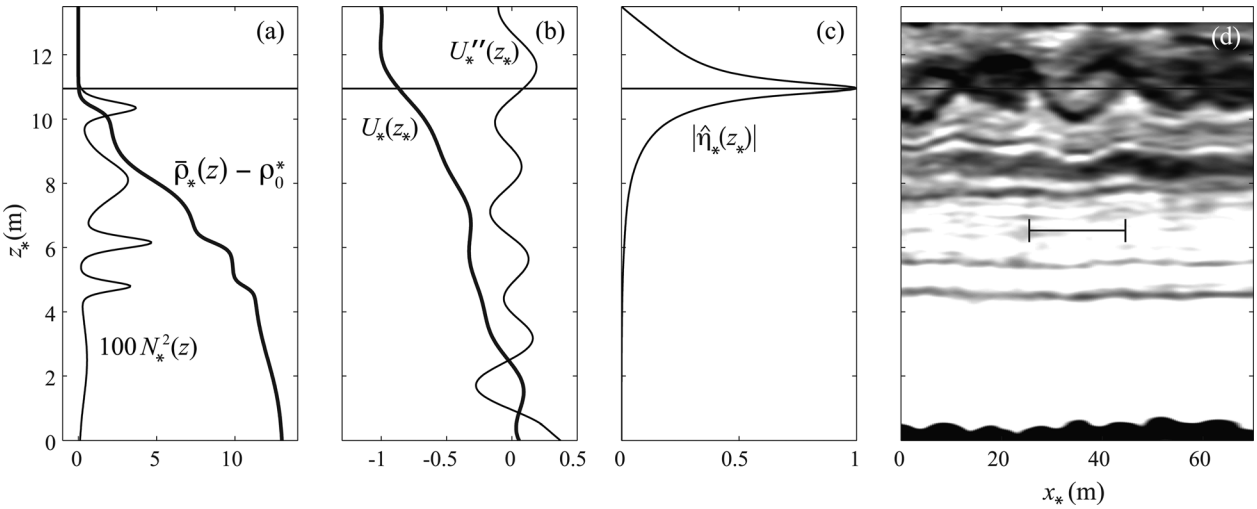

Fig. 18 Profiles measured in the Fraser River estuary. (*a*) Density and N_*^2, (*b*) velocity and vorticity gradients, along with the displacement eigenfunction from the most amplified wavenumber of the linear stability predictions in (*c*). An echosounding image is shown in (*d*) where instability waves can be seen at the depth where the eigenfunction predicts a maximum displacement (indicated by the horizontal line in all panels). The wavelength of maximum growth rate is shown by the horizontal bar in (*d*). (Figure is modified from Tedford et al. [45].)

smooth profiles is that it opens the possibility to study geophysical flows. However, these flows are often found to be considerably more complex, and we have thus far focused only on very simple profiles that are composed of a few identifiable interfaces, or interfacial regions. In this section, we look at an example of a set of profiles taken from the Fraser River estuary in British Columbia, Canada (Fig. 18, see Tedford et al. [45] for further details). Both the U_* and $\bar{\rho}_*$ profiles are composed of many interfacial regions, as seen by the extrema in U_*'' and N_*^2, and allows for many possible unstable interactions between these interfaces. Indeed, waveforms that resemble shear instabilities were observed in this region by an echosounder, and can be seen in Fig. 18(*d*). In addition to the complexity of this flow, there are many additional processes that may be acting to influence the state of the vorticity and internal waves such as topographic features, wind forcing, and a changing mean flow, to name a few.

It is encouraging, however, that the linear theory appears to be capable of predicting the occurrence and essential characteristics of stratified shear instabilities in such a large-scale geophysical flow [45]. Figure 18(*c*) shows the vertical displacement eigenfunction of the most amplified wavenumber predicted from the linear stability analysis. The depth of maximum displacement coincides with the depth of the unstable waves in the echosounding image (Fig. 18(*d*)), and the wavelength of maximum growth, shown as the horizontal bar in Fig. 18(*d*), is also found to be in agreement with the observations.

These results give us confidence that the linear theory is capable of capturing the essential dynamics of the instability process. This led Carpenter et al. [27] to go one step further and analyze the wave interactions in this flow. They found that all but three of the interfacial regions present in the profiles could be neglected when accounting for the growth of the instability, suggesting that it is due to only these three interacting waves. The dominant mechanism of instability is a Holmboe interaction between the uppermost vorticity interface (just below 12 m) and the uppermost density interface (just above 10 m), but there is also a smaller KH interaction. They also suggested that the mechanism of instability, as described by the wave interactions, may be used as a guide to predicting the nonlinear behavior of the flow. Although it is difficult to interpret echosounding images in detail, the structures in Fig. 18(*d*) appear as the cusplike internal waves that are characteristic of Holmboe's instability [46–48].

6 Summary and Outlook

In this paper, we have described an interpretation of the mechanism of stratified shear flow instability in terms of interacting waves. The great advantage of this interpretation is that it gives one a physically-based understanding of the often nonintuitive results from a stability analysis. Every effort has been made to keep the mathematical details as simple as possible, and this has generally limited discussion to piecewise profiles of velocity and density. However, we emphasize that these piecewise profiles often contain the same basic mechanisms as the smooth profiles, and can be used to understand many topics, from Rayleigh's inflection point theorem to identifying instabilities in geophysical flows. We have focused on giving the reader an introduction to the theory, while reviewing much of the essential literature that the theory is based on.

Research on the wave interaction interpretation is ongoing, and recent studies that have not been discussed in this paper have focused on various applications and extensions to the basic theory presented here. A notable application is the use of the piecewise shear layer to provide a simple understanding of optimal transient growth in homogeneous shear flow [19]. This involves accounting for the time-dependent interactions between vorticity waves from an arbitrary initial condition, and is able to explain the large transient growth rates that may occur.

Perhaps the most pressing unsolved problem is an interpretation of the Miles–Howard theorem [49,50] in terms of wave interactions. In the homogeneous case, the Rayleigh and Fjørtoft conditions result directly from domain-integrated constants of motion—the pseudomomentum and pseudoenergy, respectively [11]. In contrast, it is not known whether the Miles–Howard condition can be derived from another constant of motion in a stratified flow. Recent progress in this area has come from Rabinovich et al. [29] in their analysis of the Taylor–Caulfield-type interaction of two internal gravity waves. By allowing for an ambient density gradient, as well as two density interfaces, they were able to observe the stabilization of the TC interaction once the Miles–Howard necessary condition was no longer satisfied. They attribute this stabilization to the development of a critical layer (in which $U = c_r$ at some level in the profiles), and analyze its effect by the same wave interaction principles used for piecewise profiles. It is possible that future work could provide a single unifying

description of stratified shear flow instability that includes an interpretation of the critical layer view [1] as well.

Ultimately, it is the nonlinear evolution of the instabilities that is of concern, and this discussion of the linear problem constitutes a necessary step in this direction. Since it is known that different linear growth mechanisms can lead to very different nonlinear instabilities, a knowledge of the linear problem is most helpful in determining important nonlinear properties of instabilities, such as turbulence levels and the ensuing scalar mixing. One example is in the behavior of KH- and H-type instabilities: the former is known to produce stationary overturning billows [51,52], whereas the latter consists of propagating cusplike waves [46–48]. These very different nonlinear forms have been linked to different scalar mixing behaviors [53–55], and it is likely that a knowledge of the mechanism of instability is required for a full description of the mixing process. With the ability to assess the different instability mechanisms that are present in large-scale geophysical flows, we may begin to evaluate the importance of the three fundamental interaction types (KH, H, and TC). Further work in this direction will provide a description (or parameterization) of mixing processes in terms of the instability mechanisms.

Acknowledgment

We would like to thank Neil Balmforth and Anirban Guha for helpful discussions. This work was partially supported by NSERC. Eyal Heifetz is grateful for the Rossby visiting fellowship of the International Meteorological Institute (IMI) of Sweden.

References

[1] Lindzen, R., 1988, "Instability of Plane Parallel Shear Flow (Toward a Mechanistic Picture of How it Works)," PAGEOPH, **126**, pp. 103–121.
[2] Drazin, P., and Reid, W., 1982, *Hydrodynamic Stability*, Cambridge University Press, Cambridge, UK.
[3] Betchov, R., and Criminale, W., 1967, *Stability of Parallel Flows*, Academic Press, New York.
[4] Schmid, P., and Henningson, D., 2001, *Stability and Transition in Shear Flows*, Springer, New York.
[5] Koppel, D., 1964, "On the Stability of a Thermally Stratified Fluid Under the Action of Gravity," J. Math. Phys., **5**, pp. 963–982.
[6] Smyth, W., and Peltier, W., 1991, "Instability and Transition in Finite-Amplitude Kelvin-Helmholtz and Holmboe Waves," J. Fluid Mech., **228**, pp. 387–415.
[7] Chagelishvili, G. D., Khujadze, G. R., Lominadze, J. G., and Rogava, A. D., 1997, "Acoustic Waves in Unbounded Shear Flows," Phys. Fluids, **9**(7), pp. 1955–1962.
[8] Alexakis, A., Young, Y., and Rosner, R., 2002, "Shear Instability of Fluid Interfaces: Stability Analysis," Phys. Rev. E, **65**, p. 026313.
[9] Umurhan, O., and Heifetz, E., 2007, "Holmboe Modes Revisited," Phys. Fluids, **19**, p. 064102.
[10] Bretherton, F., 1966, "Baroclinic Instability and the Short Wavelength Cut-Off in Terms of Potential Vorticity," Q. J. R. Meteorol. Soc., **92**, pp. 335–345.
[11] Heifetz, E., Bishop, C., Hoskins, B., and Methven, J., 2004, "The Counter-Propagating Rossby-Wave Perspective on Baroclinic Instability. I: Mathematical Basis," Q. J. R. Meteorol. Soc., **130**, pp. 211–231.
[12] Smyth, W., and Peltier, W., 1990, "Three-Dimensional Primary Instabilities of a Stratified, Dissipative, Parallel Flow," Geophys. Astrophys. Fluid Dyn., **52**, pp. 249–261.
[13] Gelfgat, A. Y., and Kit, E., 2006, "Spatial Versus Temporal Instabilities in a Parametrically Forced Stratified Mixing Layer," J. Fluid Mech., **552**, pp. 189–227.
[14] Holmboe, J., 1962, "On the Behavior of Symmetric Waves in Stratified Shear Layers," Geofys. Publ., **24**, pp. 67–112.
[15] Baines, P., and Mitsudera, H., 1994, "On the Mechanism of Shear Flow Instabilities," J. Fluid Mech., **276**, pp. 327–342.
[16] Kundu, P., Cohen, I., and Hu, H., 2004, *Fluid Mechanics*, 2nd ed., Elsevier, Amsterdam.
[17] Caulfield, C., 1994, "Multiple Linear Instability of Layered Stratified Shear Flow," J. Fluid Mech., **258**, pp. 255–285.
[18] Heifetz, E., Bishop, C. H., and Alpert, P., 1999, "Counter-Propagating Rossby Waves in the Barotropic Rayleigh Model of Shear Instability," Q. J. R. Meteorol. Soc., **125**, pp. 2835–2853.
[19] Heifetz, E., and Methven, J., 2005, "Relating Optimal Growth to Counterpropagating Rossby Waves in Shear Instability," Phys. Fluids, **17**, p. 064107.
[20] Heifetz, E., Reuveni, Y., Gelfgat, A., Kit, E., and Methven, J., 2006, "Counterpropagating Rossby Wave Perspective on Kelvin Helmholtz Instability as a Limiting Case of a Rayleigh Shear Layer With Zero Width," Phys. Fluids, **18**, p. 018101.
[21] Farrell, B., 1988, "Optimal Excitation of Perturbations in Viscous Shear Flow," Phys. Fluids, **31**, pp. 2093–2101.
[22] Rayleigh, J., 1880, "On the Stability, or Instability, of Certain Fluid Motions," Proc. Lond. Math. Soc., **12**, pp. 57–70.
[23] Garcia, R., 1956, "Barotropic Waves in Straight Parallel Flow With Curved Velocity Profile," Tellus, **8**, pp. 82–93.
[24] Baines, P., 1995, *Topographic Effects in Stratified Flows*, Cambridge University Press, Cambridge, UK.
[25] Michalke, A., 1964, "On the Inviscid Instability of Hyperbolic-Tangent Velocity Profile," J. Fluid Mech., **19**, pp. 543–556.
[26] Hazel, P., 1972, "Numerical Studies of the Stability of Inviscid Stratified Shear Flows," J. Fluid Mech., **51**, pp. 39–61.
[27] Carpenter, J., Balmforth, N., and Lawrence, G., 2010, "Identifying Unstable Modes in Stratified Shear Layers," Phys. Fluids, **22**, p. 054104.
[28] Harnik, N., Heifetz, E., Umurhan, O., and Lott, F., 2008, "A Buoyancy-Vorticity Wave Interaction Approach to Stratified Shear Flow," J. Atmos. Sci., **65**, pp. 2615–2630.
[29] Rabinovich, A., Umurhan, O., Harnik, N., Lott, F., and Heifetz, E., 2011, "Vorticity Inversion and Action-at-a-Distance Instability in Stably Stratified Shear Flow," J. Fluid Mech., **670**, pp. 301–325.
[30] Balmforth, N. J., Roy, A., and Caulfield, C. P., 2012, "Dynamics of Vorticity Defects in Stratified Shear Flow," J. Fluid Mech., **694**, pp. 292–331.
[31] Craik, A., 1985, *Wave Interactions and Fluid Flows*, Cambridge University Press, Cambridge, UK.
[32] Cairns, R., 1979, "The Role of Negative Energy Waves in Some Instabilities of Parallel Flows," J. Fluid Mech., **92**, pp. 1–14.
[33] Fjørtoft, R., 1950, "Application of Integral Theorems in Deriving Criteria of Stability of Laminar Flows and for the Baroclinic Circular Vortex," Geofys. Publ., **17**, pp. 1–52.
[34] Drazin, P., 2002, *Introduction to Hydrodynamic Stability*, 1st ed., Cambridge University Press, Cambridge, UK.
[35] Howard, L., and Maslowe, S., 1973, "Stability of Stratified Shear Flows," Boundary-Layer Meteorol., **4**, pp. 511–523.
[36] Redekopp, L., 2001, "Elements of Instability Theory for Environmental Flows," *Environmental Stratified Flows*, Kluwer, Boston.
[37] Harnik, N., and Heifetz, E., 2007, "Relating Overreflection and Wave Geometry to the Counterpropagating Rossby Wave Perspective: Toward a Deeper Understanding of Shear Instability," J. Atmos. Sci., **64**, pp. 2238–2261.
[38] Taylor, G., 1931, "Effect of Variation in Density on the Stability of Superposed Streams of Fluid," Proc. R. Soc. Lond. A, **132**, pp. 499–523.
[39] Caulfield, C., Peltier, W., Yoshida, S., and Ohtani, M., 1995, "An Experimental Investigation of the Instability of a Shear Flow With Multilayered Density Stratification," Phys. Fluids, **7**, pp. 3028–3041.
[40] Kelvin, W., 1871, "Hydrokinetic Solutions and Observations," Philos. Mag., **42**, pp. 362–377.
[41] Helmholtz, H., 1868, "On Discontinuous Movements of Fluids," Philos. Mag., **36**, pp. 337–346.
[42] Lawrence, G., Browand, F., and Redekopp, L., 1991, "The Stability of a Sheared Density Interface," Phys. Fluids, **3**(10), pp. 2360–2370.
[43] Alexakis, A., 2005, "On Holmboe's Instability for Smooth Shear and Density Profiles," Phys. Fluids, **17**, p. 084103.
[44] Haigh, S., and Lawrence, G., 1999, "Symmetric and Nonsymmetric Holmboe Instabilities in an Inviscid Flow," Phys. Fluids, **11**(6), pp. 1459–1468.
[45] Tedford, E., Carpenter, J., Pawlowicz, R., Pieters, R., and Lawrence, G., 2009, "Observation and Analysis of Shear Instability in the Fraser River Estuary," J. Geophys. Res., **114**, p. C11006.
[46] Smyth, W., Klaassen, G., and Peltier, W., 1988, "Finite Amplitude Holmboe Waves," Geophys. Astrophys. Fluid Dyn., **43**, pp. 181–222.
[47] Zhu, D., and Lawrence, G., 2001, "Holmboe's Instability in Exchange Flows," J. Fluid Mech., **429**, pp. 391–409.
[48] Tedford, E., Pieters, R., and Lawrence, G., 2009, "Symmetric Holmboe Instabilities in a Laboratory Exchange Flow," J. Fluid Mech., **636**, pp. 137–153.
[49] Miles, J., 1961, "On the Stability of Heterogeneous Shear Flows," J. Fluid Mech., **10**, pp. 496–508.
[50] Howard, L., 1961, "Note on a Paper of John W. Miles," J. Fluid Mech., **10**, pp. 509–512.
[51] Thorpe, S., 1973, "Experiments on Instability and Turbulence in a Stratified Shear Flow," J. Fluid Mech., **61**, pp. 731–751.
[52] Caulfield, C., and Peltier, W., 2000, "The Anatomy of the Mixing Transition in Homogenous and Stratified Free Shear Layers," J. Fluid Mech., **413**, pp. 1–47.
[53] Smyth, W., and Winters, K., 2003, "Turbulence and Mixing in Holmboe Waves," J. Phys. Oceanogr., **33**, pp. 694–711.
[54] Smyth, W., Carpenter, J., and Lawrence, G., 2007, "Mixing in Symmetric Holmboe Waves," J. Phys. Oceanogr., **37**, pp. 1566–1583.
[55] Carpenter, J., Lawrence, G., and Smyth, W., 2007, "Evolution and Mixing of Asymmetric Holmboe Instabilities," J. Fluid Mech., **582**, pp. 103–132.